APPLICATIONS OF LOGVINENKO'S COLOUR ATLAS

by

Hamidreza MIRZAEI
B.Sc. in Computer Engineering
Isfahan University of Technology, 2009

THESIS SUBMITTED IN PARTIAL FULFILLMENT OF
THE REQUIREMENTS FOR THE DEGREE OF

MASTER OF SCIENCE

In the
School of Computing Science

Faculty of Applied Sciences

SIMON FRASER UNIVERSITY

Fall 2011

APPROVAL

Name: **Hamidreza Mirzaei**

Degree: **Master of Science**

Title of Thesis: **APPLICATIONS OF LOGVINENKO'S COLOUR ATLAS**

Examining Committee:

Dr. Ze-Nian Li
Chair

Dr. Brian Funt
Senior Supervisor
Professor

Dr. Art Liestman
Supervisor
Professor

Dr. Alexander Logvinenko
External Examiner
Professor
Glasgow Caledonian University, Glasgow, UK

Date Defended/Approved: 13 September 2011

Declaration of
Partial Copyright Licence

ABSTRACT

Alexander Logvinenko has recently introduced a new colour atlas based on idealized reflectances called rectangular metamers. In this thesis, the Gaussian parameterization of Logvinenko's colour atlas has been implemented, allowing us to investigate its interesting features, of which, illumination invariance is of most importance. The new colour descriptors are employed for predicting illuminant-induced colour stimulus changes, because these coordinates in the atlas specify reflectances; and, as such, they can be computationally 'relit' using the spectrum of the second illuminant. The superiority of the new approach over other methods is revealed in experimental results. Furthermore, Logvinenko's theory provides a structure in which a complete set of colour equivalent material and illumination pairs can be generated to match any given input RGB. The set of such pairs defines a material-lighting-invariance manifold, based on which, a new illumination-estimation method is proposed, which calculates the intersection of the manifolds through a Hough-like voting process.

Keywords: Colour Space; Colour Stimulus Prediction; Colour Constancy; Wraparound Gaussians.

ACKNOWLEDGEMENTS

This dissertation would not have been possible without the guidance and the help of several individuals who in one way or another contributed and extended their valuable assistance in the preparation and completion of this study. First and foremost, my utmost gratitude goes to Dr. Brian Funt, for his inspirations and guidance throughout my research. I am also indebted to my supervisor, Art Liestman, for his support. A special thanks also goes to Alexander Logvinenko for his enthusiasm on the subject, his bright ideas, and his helpful comments. Lastly, and most importantly, I wish to thank my parents for their continual support and love. I dedicate this thesis to them.

TABLE OF CONTENTS

LIST OF FIGURES

LIST OF TABLES

1: GAUSSIAN PARAMETERIZATION OF LOGVINENKO'S COLOUR-ATLAS

1.1 An Introduction to ADL Colour Space

Common colour spaces used in the literature of Colour Science, such as CIE 1931 and its derivatives, are more appropriate for representing self-luminous than reflecting objects. The main problem is that they may work well for a fixed illumination, but can lead to unsatisfactory results under illumination change. Traditionally, the colour signal produced by a surface with reflectance spectrum $S(\lambda)$ illuminated by a light with spectral power distribution $E(\lambda)$ is defined as

$$\varphi_i = \int_{\lambda_{\min}}^{\lambda_{\max}} E(\lambda)S(\lambda)R_i(\lambda)d\lambda \qquad i = 1,2,3$$

where $R_i(\lambda)$ is the spectral sensitivity function of the sensors and $[\lambda_{min}, \lambda_{max}]$ indicates the visible wavelength interval. Given a fixed illumination, the reflecting objects producing the same colour signal (metameric reflecting objects) will have the same colour. However, when the illumination is changed, two metameric reflecting objects under the first illuminant may no longer produce the same colour signal under the second. On the other hand, there may be reflecting surfaces, which produce different colour signals under one illuminant, while they are metameric under another illuminant [1]. Indeed, some reflecting objects will continue to be in the same metameric class by the change of illumination, while some others will not [1].

Logvinenko introduces a colour atlas in order to represent the colour of objects [1]. He defines a colour atlas as a set of non-metameric spectral reflectance functions under a given illuminant [1]. Each element of a colour atlas can be viewed as representing an equivalence class of metameric reflectances; a complete colour atlas is a one that includes all the possible metameric classes. Since the metameric classes may change with a change of illumination, when talking about a colour atlas, it is necessary to consider the set of illuminants for which the given set of spectral reflectance functions is a colour atlas [1]. When the same set of spectral reflectance functions is a colour atlas for a set of illuminants, this colour atlas is called invariant with respect to that illuminant family. The key issue is that no two reflectances in the atlas that are non-metameric under one illuminant become metameric under a second illuminant from the illuminant family. Logvinenko's atlas is invariant under all strictly positive illuminants. In his proposed colour atlas, when illumination changes, the equivalence classes of reflectances that are metameric to an element of the atlas may change, but the underlying set of reflectances does not. In other words, the atlas can uniquely represent the metameric classes independent of the illumination [1]. In this chapter we are going to investigate this colour space and its Gaussian representation.

Given an illuminant with the spectral power distribution $E(\lambda)>0$, for each spectral reflectance function $S(\lambda)$ there is a unique optimal spectral reflectance function $S_{opt}(\lambda)$ and a unique number $0\leq \alpha \leq 1$ such that spectral reflectance function

$(1- \alpha).x_{0.5}(\lambda) + \alpha. x_{opt}(\lambda)$

with $x_{0.5}(\lambda)$=0.5 is metameric to $S(\lambda)$. This provides Logvinenko with the basic vehicle to propose his colour atlas theory.

The optimal spectral reflectance functions can take only two values: 0 or 1. For example, a step function with transition at wavelength λ_1 defined as

$x_1(\lambda;\lambda_1)=0$ *if* $(\lambda \leq \lambda_1)$ *and 1 otherwise*

or the spectral reflectance function defined as

$x(\lambda) = 1$

are two examples of optimal functions.

Logvinenko bases his colour atlas on the generally accepted assumption that optimal colour stimuli, i.e., the object-colour stimuli that for a given chromaticity have the greatest purity, are generated by an either 0 or 1 spectra with no more than two transitions across the visible wavelength range [2]. Therefore if the two-transition property holds true, the optimal spectral reflectance function can be specified by two transition wavelengths, λ_1 *and* λ_2*:*

$x_2(\lambda;\lambda_1, \lambda_2) = x_1(\lambda;\lambda_1) - x_1(\lambda;\lambda_2)$

Note that this assumption does not always hold true. In this work, however, we will mainly focus on CIE 1931 2◦ standard observer for which the optimal reflectance functions are two-transition spectra [3]. He then defines an *object-colour solid* as the set of possible colours of reflecting objects and describes the optimal points on the surface of the object-colour solid. The illuminant must be positive everywhere in order to satisfy the two-transition property. It has been also shown that the points on the surface are unique, i.e., they can be uniquely defined by two transition wavelengths specified as λ_1 and λ_2[1].

In summary, in Logvinenko's theory, the object reflectances and light spectra can be represented in terms of rectangular functions [1] that are a mixture of uniform gray and a rectangular component that takes only values 0 and 1, with at most 2 transitions between 0 and 1. Given λ_1 and λ_2 as transition wavelengths, it is also possible to express the optimal reflectance functions by a central wavelength λ and a spectral bandwidth δ. Therefore, the colour atlas is based on idealized reflectances called rectangular metamers that are specified by 3 parameters: α (chromatic amplitude), δ (spectral bandwidth) and λ (central wavelength).

This colour space has several interesting features including illumination invariance, reasonable correlation of its coordinate axes with perceptual dimensions, and the possibility of predicting the effects of a change in illuminant colour based on its rectangular metamer reflectances. Another favourable property is that the colour descriptors do not vary too much with a change of colour matching functions. In particular, they do not change at all with linear transformations of the sensitivities.

Starting from the rectangular colour atlas, one can specify the object colour atlas with various parameterizations. Inspired by the usefulness of the Gaussian functions in defining objects' and lights' spectral functions in the literature [4][5], one can utilize them to represent the whole colour stimulus set of Logvinenko.

1.2 Gaussian Parameterization

Consider a three-parameter set of spectral reflectance functions $g_m(\lambda;k_m,\theta_m,\mu_m)$, and a similar three-parameter set of spectral power distribution functions $g_l(\lambda;k_l,\theta_l,\mu_l)$, both of which are Gaussian-like functions where k, θ, and μ indicate the height, standard

deviation and center (peak wavelength) of the Gaussian. These functions are not strictly Gaussians, but rather are defined on a finite wavelength interval $[\lambda_{\min},\lambda_{\max}]$ and in some cases wraparound at the ends of the interval. Spectra of this type have been called "wraparound Gaussians" [6]. Following Logvinenko [7], wraparound Gaussians are defined by equations 1 to 4.

If $\mu_m \le (\lambda_{\max} + \lambda_{\min})/2$ we have two cases:

1. For $\lambda_{\min} \le \lambda \le \mu_m + \Lambda/2$:

$$g_m(\lambda;k_m,\theta_m,\mu_m) = k_m \exp[-\theta_m(\lambda - \mu_m)^2]; \quad (1)$$

2. For $\mu_m + \Lambda/2 \le \lambda \le \lambda_{\max}$:

$$g_m(\lambda;k_m,\theta_m,\mu_m) = k_m \exp[-\theta_m(\lambda - \mu_m - \Lambda)^2]; \quad (2)$$

where $\Lambda = \lambda_{\max} - \lambda_{\min}$.

On the other hand when $\mu_m \ge (\lambda_{\max} + \lambda_{\min})/2$, again we have two cases:

1. For $\lambda_{\min} \le \lambda \le \mu_m - \Lambda/2$

$$g_m(\lambda;k_m,\theta_m,\mu_m) = k_m \exp[-\theta_m(\lambda - \mu_m + \Lambda)^2]; \quad (3)$$

2. For $\mu_m - \Lambda/2 \le \lambda \le \lambda_{\max}$

$$g_m(\lambda;k_m,\theta_m,\mu_m) = k_m \exp[-\theta_m(\lambda - \mu_m)^2]; \quad (4)$$

Then, for $0 \le k_m \le 1$, $\lambda_{\min} \le \mu \le \lambda_{\max}$ and positive θ_m, we have a Gaussian for reflectance spectra. The Gaussians for illuminant spectral power distributions are defined similarly except ($0 \le k_l$). In this representation, μ and θ correspond in their roles to the

central wavelength λ and the spectral bandwidth δ as defined in the Logvinenko's original [1] αδλ coordinate system. We will refer to the triple $k\theta\mu$ as the KSM[1] coordinates. Note that Logvinenko's wraparound Gaussians are not the same as the inverse Gaussians defined by Golz [5].

Figure 1.1 shows an example of a Gaussian metamer and a rectangular metamer for a sample Munsell chip.

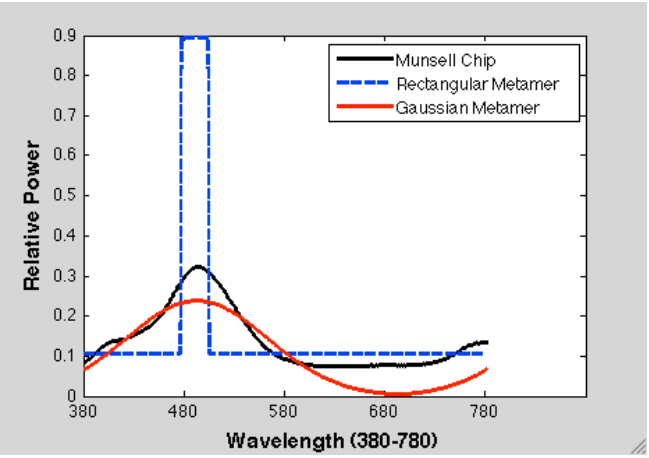

Figure 1.1 A sample Munsell chip's spectral reflectance illuminated by D65 and its rectangular and Gaussian metamers shown by black, blue and red respectively.

1.3 Calculating Colour Descriptors by Optimization

The first part of this thesis is motivated by the shortcoming of the direct method of colour descriptor calculation presented in [1] in terms of speed. The direct method for calculating the colour descriptors involves a search in a 3-dimensional parameter space

[1] S stands for Standard deviation, and M stands for Peak Wavelength.

and is computationally expensive. To address this issue, in this work we have proposed a 2-dimensional optimization method using interpolation, which reduces the computational time significantly. This method is easy to put into practice and we have implemented and made it available online. [2]

Computing the Gaussian metamer parameters is analogous to computing those of rectangular metamers. We have applied the same basic interpolation approach as developed by Godau et al. [8] for that case.

In order to find the KSM colour descriptors corresponding to a set of sensor responses φ_0 under a given illumination with the spectral power distribution *E(λ)*, one can find the KSM such that the angular difference (equation 6) between the resulting sensor response $\varphi(K,S,M)$ and φ_0 (equation 7) is minimized.

$$\varphi(K,S,M) = \int_{\lambda_{\min}}^{\lambda_{\max}} E(\lambda)S(\lambda;K,S,M)R_i(\lambda)d\lambda \qquad i = 1,2,3 \tag{5}$$

$$AngularDifference(\varphi_1,\varphi_2) = \arccos\frac{\varphi_1 \cdot \varphi_2}{|\varphi_1||\varphi_2|} \tag{6}$$

$$E(K,S,M) = \arccos\frac{\varphi_0 \cdot \varphi(K,S,M)}{|\varphi_0||\varphi(K,S,M)|} \tag{7}$$

where *S(λ)* is given by the equations 1-4, and $R_i(\lambda)$ is the spectral sensitivity function of the sensor. This requires a 3-dimensional optimization. Although it is possible to minimize *E* directly, this suffers from lengthy computation. It takes several hours to calculate the KSM coordinates for the set of 1600 glossy Munsell chips (available at [9])

[2] http://www.cs.sfu.ca/~colour/code/

using the direct method. The key to success in reducing the time needed for optimization is finding starting points close enough to the solution. Following Godau et al. [8], we approach this problem using interpolation. It is possible to calculate colour stimuli for a number of samples in the KSM space. One can do this backwards as well to approximate KSM coordinates from colour stimuli. However, this still requires a rather lengthy calculation if we want to cover the whole range of possible KSM values. Therefore, there is a trade off between the computational cost of interpolation and approximation precision.

Since the angular error does not depend on the scale factor *K*, it turns out it is possible to reduce the KSM space from three to two dimensions by only considering colours on the colour-solid boundary, i.e., where *K = 1*. This way we make it convenient to use interpolation to find good starting values for *S* and *M*.

Once the starting point is reached, further optimization can then be performed if necessary to reduce the angular error defined in equation 5. However, in a few cases there is a need to restart the optimization process by randomly varying the starting values in order to find a good solution:

$$(S,M) = \arg\min_{S,M} E(1,S,M)$$

Afterwards, given *S* and *M*, the scaling *K* can be calculated directly:

$$K = \frac{|\varphi_0|}{|\varphi(1,S,M)|}$$

Eventually, the resulting KSM describes a Gaussian reflectance spectrum that is metameric to the colour stimulus φ_0 under the given illuminant.

1.4 KSM in Practice

The proposed algorithm for calculating KSM coordinates is considerably faster than direct optimization. Of course the speed of calculation depends on the required precision and the size of the data set and there is a trade off between precision and speed. The more time we spend on creating interpolation functions, generally the faster the calculation. Note, however, that it is the case up only to a certain number of interpolation points provided for creating the functions and afterwards it is not possible to achieve more speed up by spending more time on creating the functions based on smaller step sizes. It is worth mentioning that for repeated calculations for the same illuminant and observer, the interpolation functions need to be calculated only once, and can be stored for reuse. Performing the experiments on a 2.66 GHz Quad-Core Intel Mac Pro, for the set of 1600 glossy Munsell samples [9], the whole calculation takes about 2 minutes. Building the interpolation table requires the majority of the time. Given pre-computed interpolation functions, it takes about 20 seconds. Figure 1.2 shows the calculated KSM colour descriptors for a scene under D65 (spectral image retrieved from the Joensuu spectral database [9]).

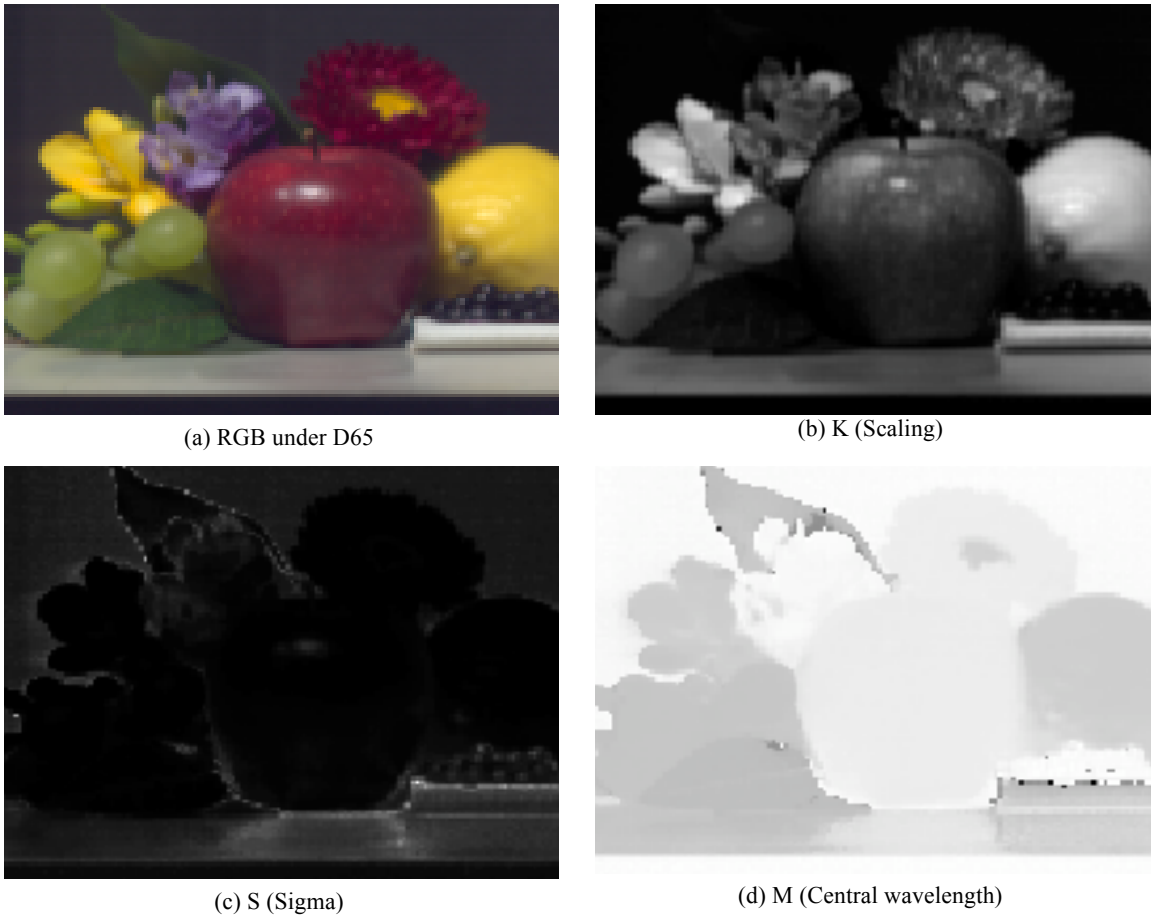

(a) RGB under D65

(b) K (Scaling)

(c) S (Sigma)

(d) M (Central wavelength)

Figure 1.2 KSM colour descriptors for a scene under D65 (spectral image retrieved from the Joensuu spectral database [9]).

1.4.1 KSM Behaviour with the Change of Illumination

One of the most helpful properties of KSM coordinates is that they show a high robustness with respect to changes in the illuminant. In an experiment, in order to show the invariance of KSM coordinates under the light changes, we synthesize the XYZ tri-stimulus values of 1600 Munsell chips under one illuminant (e.g., D65) using CIE xyz colour matching functions and find the KSM coordinates. We then find the KSM coordinates under a second illuminant (e.g., F11).

Figure 1.3 illustrates a simple comparison of the KSM coordinates for these two situations. As is clear from the figures, the colour descriptors are very similar and invariant regardless of whether F11 or D65 is used. Note that due to the wraparound property of the Gaussians, the lambda centrals near the end of the interval are in fact close to the beginning lambda centrals and so are not as different as they appear in the plots. The invariance property holds for the other illuminant pairs as well.

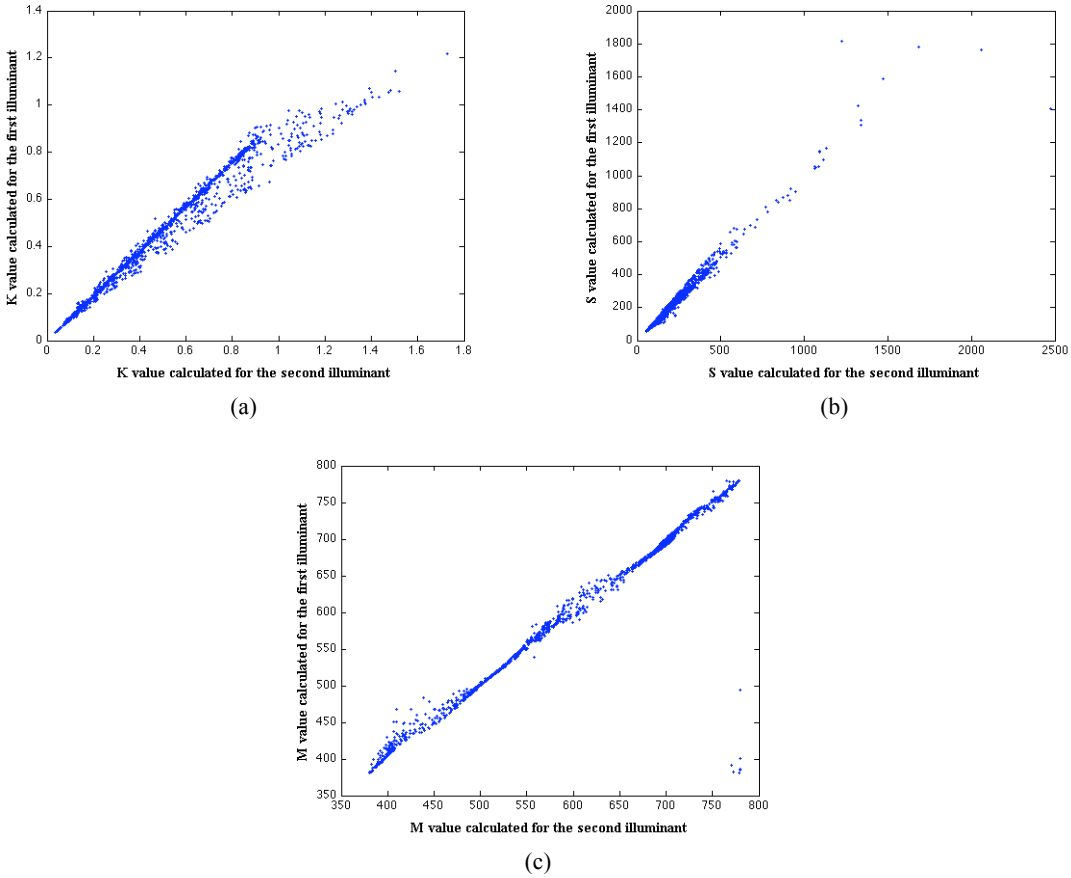

Figure 1.3 Comparison of KSM coordinates calculated under D65 and F11. (a) Comparison of K coordinates calculated under D65 and F11. (b) Comparison of S coordinates calculated under D65 and F11. (c) Comparison of M coordinates calculated under D65 and F11. Note that due to the wraparound property of the Gaussians, the lambda centrals near the upper end of the wavelength range are, in fact, still close to those at the lower end and so are not as different as they sometimes appear in the plot.

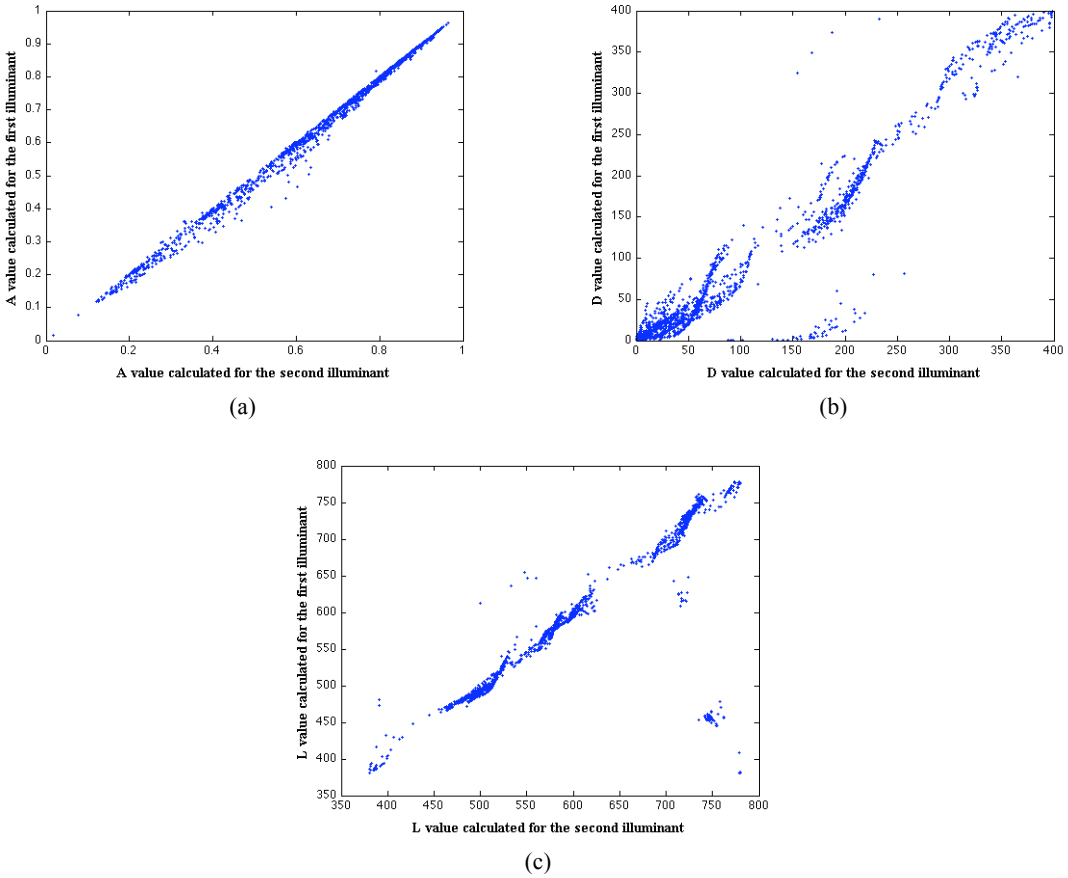

Figure 1.4 Comparison of ADL coordinates calculated under D65 and F11. (a) Comparison of A (α) values calculated under D65 and F11. (b) Comparison of D (δ) values calculated under D65 and F11. (c) Comparison of L (λ) values calculated under D65 and F11. Note that due to the wraparound property of the Gaussians, the lambda centrals near the upper end of the wavelength range are, in fact, still close to those at the lower end and so are not as different as they sometimes appear in the plot.

We also provide the same comparison for the ADL coordinates of the Munsell chips under F11 and D65. The next figure provides a plot of the corresponding ADL and KSM parameters on top of each other.

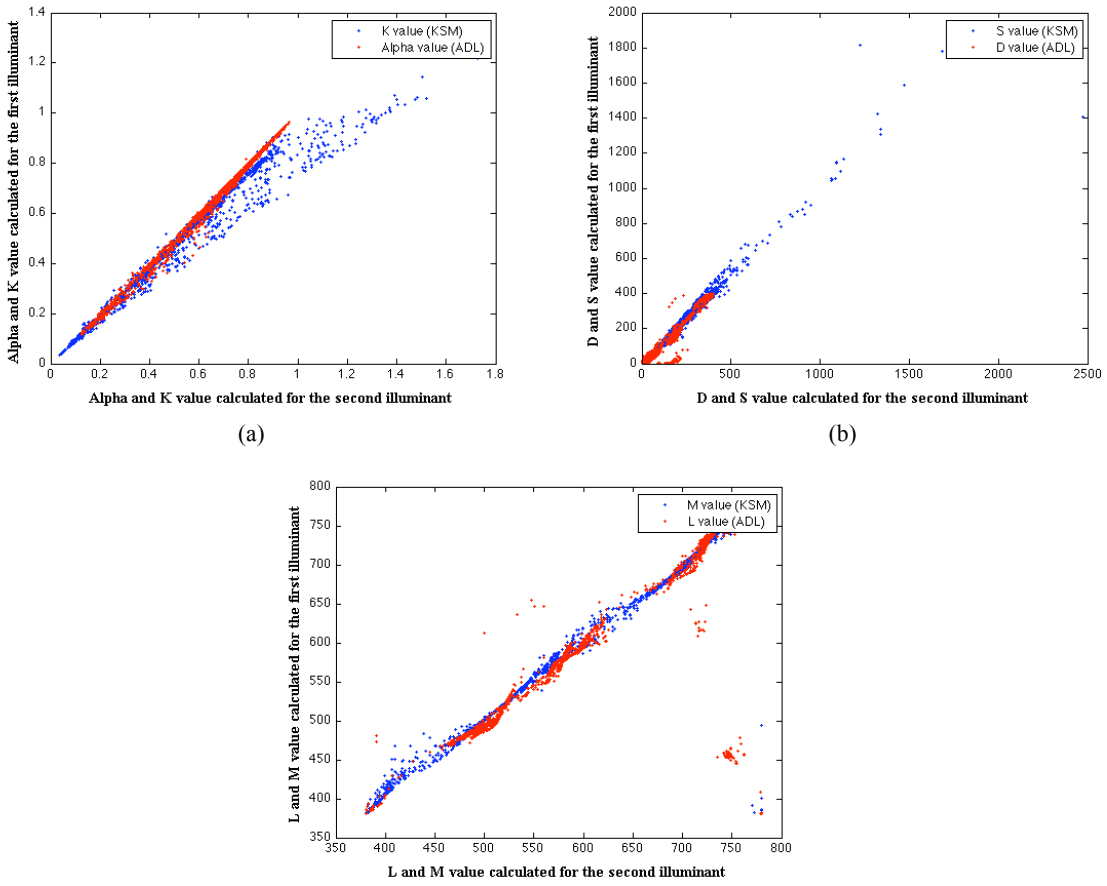

Figure 1.5 Comparison of KSM (blue points) and ADL (red points) coordinates calculated under D65 and F11. (a) Comparison of K and also A (α) values calculated under D65 and F11. (b) Comparison of S and also D (δ) values calculated under D65 and F11. (c) Comparison of M and (λ) values calculated under D65 and F11. Note that the lambda centrals near to the end of the interval are in fact close to the beginning lambda centrals.

As can be inferred from the figures, the lambda central values, which play the most important role in determining the spectra, and as claimed by Logvinenko [1] correspond to hue, are much more stable for the KSM. Indeed, although the lambda centrals cannot always be unambiguously related to hue, they can play a crucial role in determining the colour stimuli. In the next section we statistically investigate the stability

of lambda centrals under illuminant changes for KSM, ADL and also Inverse Gaussians (IG).

1.4.2 Lambda Central Stability

In order to better illustrate the stability of lambda central coordinates under illuminant changes, we compare the ADL, KSM, and also inverse Gaussians. We provide a comparison of the lambda central values calculated for glossy Munsell chips under six different illuminants introduced by Logvinenko [7]. The illuminants (numbered from 1 to 6) together with their Gaussian metamers plotted on top of them are shown in Figure 1.6. Note that although for some of the illuminants (e.g., the bottom right panel of the Figure 1.6) the Gaussian metamer curve may appear to be different from the original spectrum, they are indeed metamers. The difference is just due to the fact that the cones have very little sensitivity near the end of the visible spectrum.

We first synthesize the LMS tri-stimulus values of 1600 Munsell chips under each of the illuminants and then find the corresponding KSM, ADL and IG coordinates.

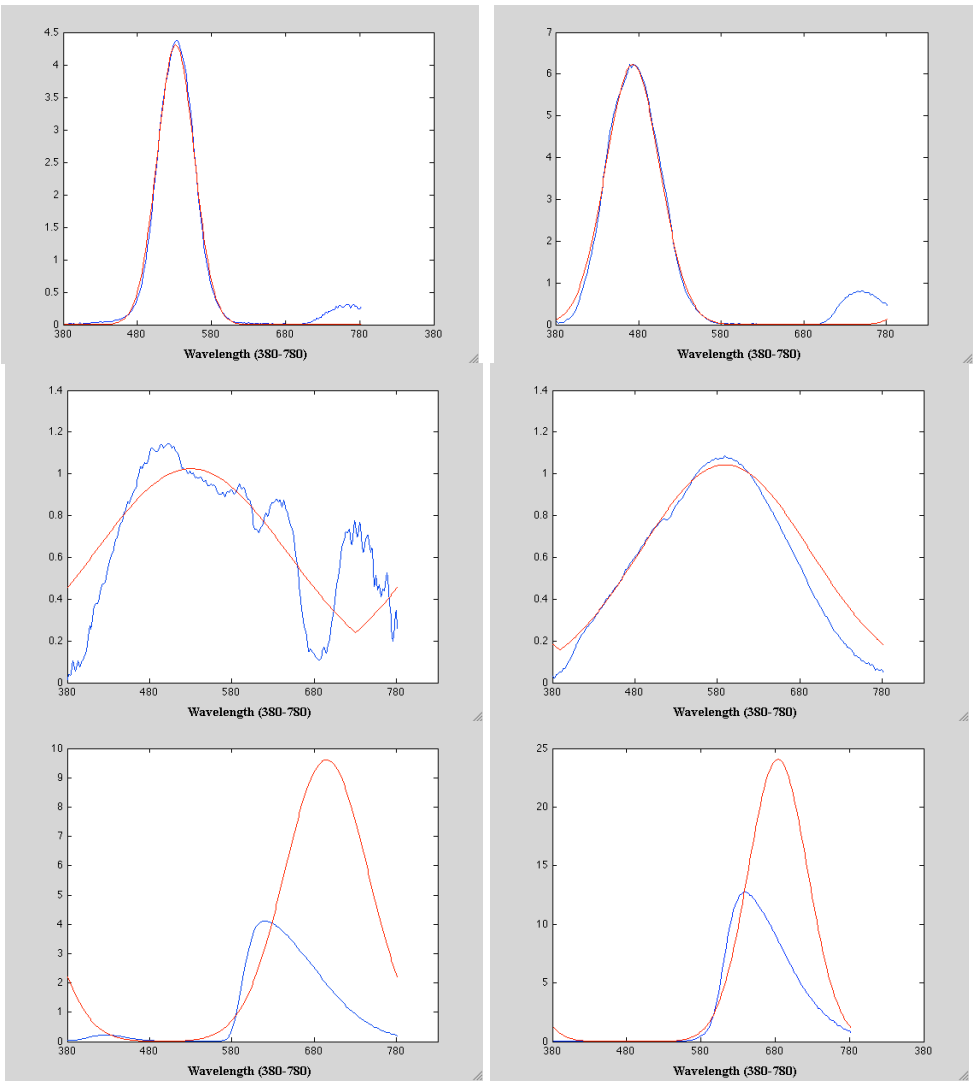

Figure 1.6 Spectra of illuminants #1 to #6 introduced by Logvinenko.

The differences of lambda centrals based on circular [10] statistics (i.e., the values near to the end of the range are close to the ones in the beginning of the range) for different colour systems, i.e., KSM, ADL and IG, are tabulated in Table 1.1. The minimums of each case are shown in bold.

Table 1.1 Differences of lambda centrals based on a circular statistic.

Illuminant Number		Median Difference			Mean Difference			Max Difference		
From	**To**	KSM	ADL	IG	KSM	ADL	IG	KSM	ADL	IG
1	**2**	**12.48**	23.22	14.42	**25.91**	46.20	46.90	**192.59**	199.57	199.94
1	**3**	14.55	20.30	**13.68**	**15.16**	31.49	17.95	173.27	174.13	**156.69**
1	**4**	**13.97**	19.70	14.01	**15.15**	33.29	19.67	**170.14**	178.53	186.45
1	**5**	**31.52**	55.89	35.48	**38.39**	60.18	57.77	**195.64**	199.48	199.67
1	**6**	**32.49**	62.63	47.19	**39.54**	62.74	68.65	**196.47**	198.52	199.77
2	**1**	**12.48**	23.22	14.42	**25.91**	46.20	46.90	**192.59**	199.57	199.94
2	**3**	**12.53**	40.12	23.35	**21.78**	55.88	51.36	**161.19**	199.80	199.86
2	**4**	**13.26**	43.34	28.33	**23.25**	58.85	55.13	**171.37**	199.03	199.47
2	**5**	**31.21**	75.66	104.27	**40.26**	76.51	98.06	**192.58**	198.75	199.79
2	**6**	**32.54**	81.95	117.72	**40.67**	81.91	105.37	**192.61**	199.77	199.87
3	**1**	14.55	20.30	**13.68**	**15.16**	31.49	17.95	173.27	174.13	**156.69**
3	**2**	**12.53**	40.12	23.35	**21.78**	55.88	51.36	**161.19**	199.80	199.86
3	**4**	**1.00**	2.58	1.37	**2.06**	4.69	5.34	**30.51**	110.44	155.92
3	**5**	**17.23**	22.08	19.15	**26.47**	35.29	45.82	188.80	**184.28**	199.77
3	**6**	**18.98**	28.20	28.39	**27.83**	42.23	58.05	**186.04**	193.37	199.83
4	**1**	**13.97**	19.70	14.01	**15.15**	33.29	19.67	**170.14**	178.53	186.45
4	**2**	**13.26**	43.34	28.33	**23.25**	58.85	55.13	**171.37**	199.03	199.47
4	**3**	**1.00**	2.58	1.37	**2.06**	4.69	5.34	**30.51**	110.44	155.92
4	**5**	**16.60**	20.58	17.64	**25.54**	32.53	42.45	189.18	**186.62**	198.36
4	**6**	**18.61**	24.96	25.71	**26.94**	38.92	54.64	**185.67**	199.08	199.56
5	**1**	**31.52**	55.89	35.48	**38.39**	60.18	57.77	**195.64**	199.48	199.67
5	**2**	**31.21**	75.66	104.27	**40.26**	76.51	98.06	**192.58**	198.75	199.79
5	**3**	**17.23**	22.08	19.15	**26.47**	35.29	45.82	188.80	**184.28**	199.77
5	**4**	**16.60**	20.58	17.64	**25.54**	32.53	42.45	189.18	**186.62**	198.36
5	**6**	**2.35**	6.45	4.38	**4.16**	13.42	12.16	**147.79**	192.64	178.47
6	**1**	**32.49**	62.63	47.19	**39.54**	62.74	68.65	**196.47**	198.52	199.77
6	**2**	**32.54**	81.95	117.72	**40.67**	81.91	105.37	**192.61**	199.77	199.87
6	**3**	**18.98**	28.20	28.39	**27.83**	42.23	58.05	**186.04**	193.37	199.83
6	**4**	**18.61**	24.96	25.71	**26.94**	38.92	54.64	**185.67**	199.08	199.56
6	**5**	**2.35**	6.45	4.38	**4.16**	13.42	12.16	**147.79**	192.64	178.47

In almost all the cases the lambda central in KSM colour system has the minimum median, average, and maximum change. Accordingly, this robustness of KSM presents an effective strategy to predict the changes in colour stimulus under illuminant changes. In the next section we investigate the behaviour of KSM coordinates under the change of observer sensitivity spectra.

1.4.3 KSM Behaviour with the Change of Observer Sensitivity Spectra

Another advantage of KSM coordinates is that they are not affected by a linear transformation of the sensors. In order to assess this property, we first synthesize the LMS tri-stimulus values of 1600 Munsell chips under one illuminant (e.g., D65) using the Stockman-Sharpe cone fundamentals [12]. We then find the KSM colour descriptors and, afterwards, synthesize the XYZ tri-stimulus values of 1600 Munsell chips under the same illuminant (i.e., D65) using CIE 1931 $\bar{x}, \bar{y}, \bar{z}$ colour matching functions, and find the corresponding KSM coordinates. The comparison of KSM colour coordinates is illustrated in Figure 1.7. Note that the few differences appeared in the plots, are due to the fact that CIE 1931 $\bar{x}, \bar{y}, \bar{z}$ colour matching functions are not precisely a linear transformation of Stockman-Sharpe cone fundamentals in practice, otherwise there must be no variation in the KSM coordinates at all.

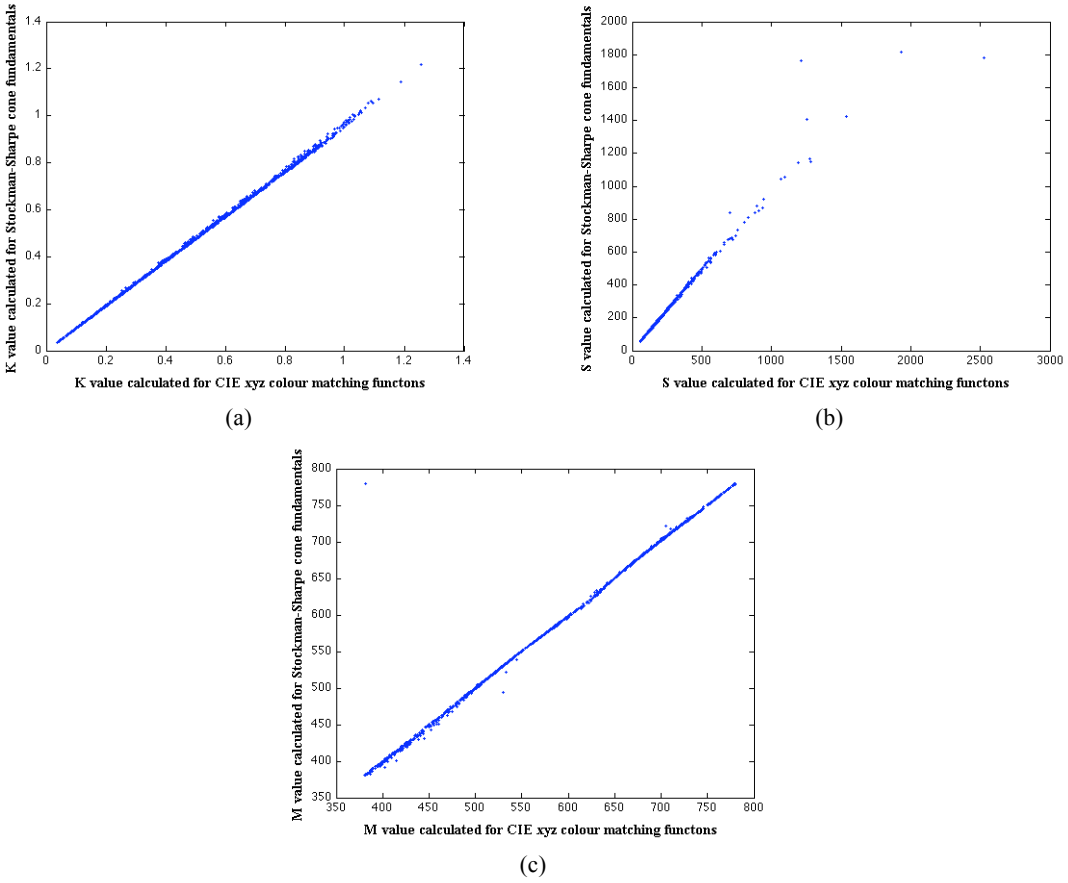

Figure 1.7 Comparison of KSM coordinates calculated under D65 for LMS colour matching functions versus for the *CIE 1931* $\bar{x},\bar{y},\bar{z}$ colour matching functions. (a) Comparison of K coordinates. (b) Comparison of S coordinates. (c) Comparison of M coordinates.

1.4.4 A Comparison of KSM vs. ADL in Terms of Their Object Colour Solid

The set of possible colour stimuli of reflecting objects specifies a volume in the space called the object-colour solid. The object-colour solid depends on the spectral power distribution of the illuminant and the employed sensor sensitivities. Figure 1.8 shows the object-colour solid for illuminant D65, in the CIE 1931 XYZ tri-stimulus space.

We compare the object colour solid obtained by KSM colour descriptors with the object colour solid yielded by ADL colour descriptors. As we can see in Figure 1.9, the KSM object colour solid lies inside the ADL one. That is because in the Gaussian representation we have limited the maximum value of the scaling K to 1, which means that the Gaussian cannot generate all the potential colour stimuli of the object-colour space as ADL coordinates do. In order to go through all those possibilities, one can go beyond the limit and have K values greater than 1, but then they will no longer represent physically realizable reflectances.

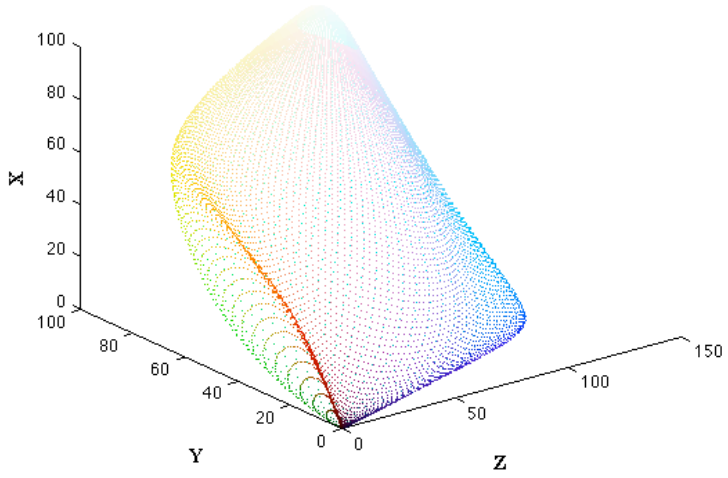

Figure 1.8 **Object-colour solid in the CIE 1931 XYZ tri-stimulus space for illuminant D65. The colour coding is approximate and roughly indicates the colours of the corresponding XYZ points.**

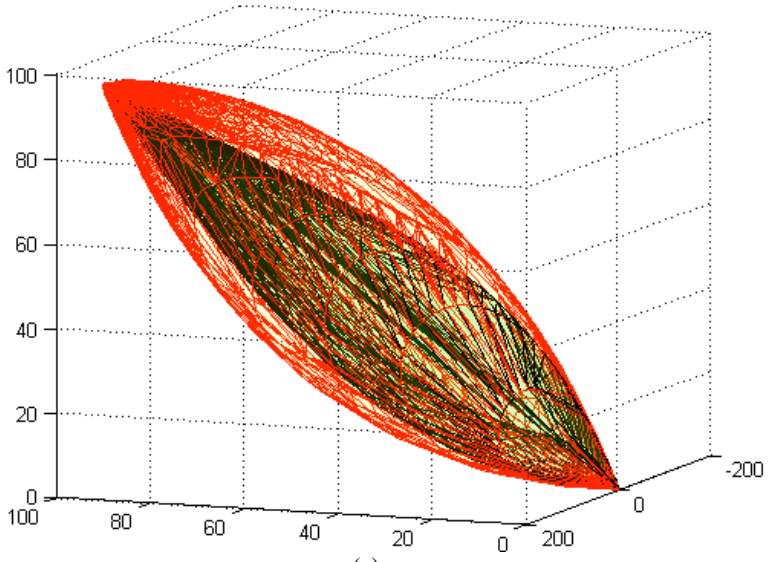

(a)

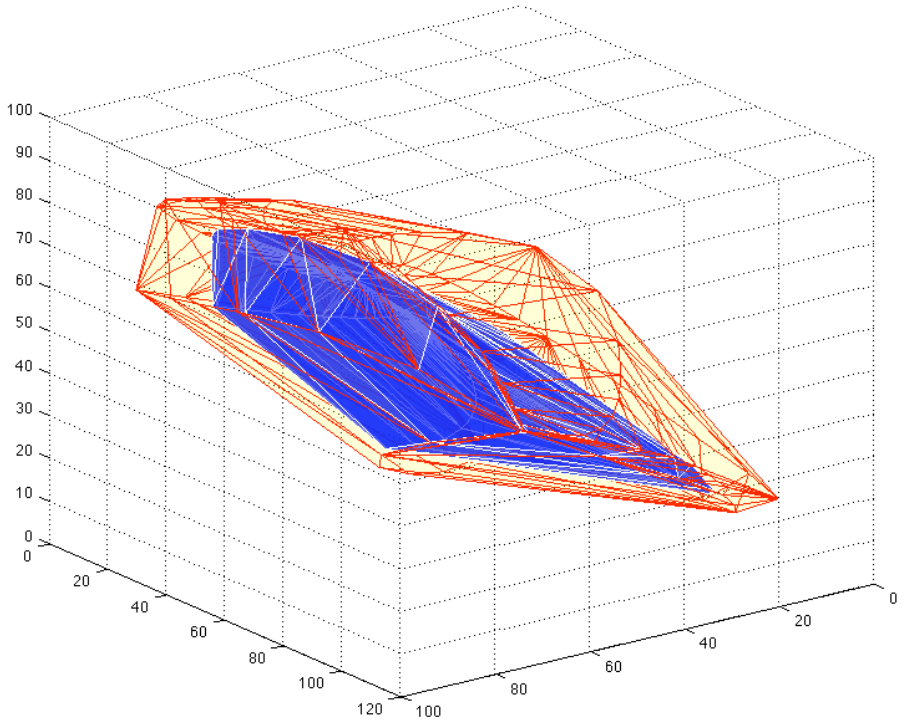

(b)

Figure 1.9 - Comparison of the object colour solid obtained by KSM with the object colour solid obtained by ADL (a) Dense sampling (b) Sparse sampling. The KSM object colour solid lies strictly within the ADL one.

1.5 Summary

In this chapter, the Gaussian representation of ADL colour space was investigated and an algorithm for converting XYZ (or LMS) colour coordinates to KSM coordinates was developed that enables us to calculate the descriptors for large data sets or images. Furthermore, measures of the change in KSM coordinates under a change of illumination or a change of the observer spectral sensitivities confirmed the invariance property KSM colour descriptors. The interesting features of this colour space enable us to put forward our contributions towards a variety of applications including colour stimulus prediction and colour constancy.

2: COLOUR STIMULUS PREDICTION

2.1 Introduction

Predicting how the colour stimulus (i.e., cone LMS, CIE XYZ or sRGB) in response to light reflected from a surface changes under changing lighting is a long-standing and important problem. It arises in white balancing digital imagery, and when re-rendering printed material for viewing under a second illuminant (e.g., changing from D65 to D50). We approach this problem from the perspective of Logvinenko's [1] new colour atlas. His proposed colour atlas is based on idealized reflectances called rectangular metamers derived from 2-transition optimal colour stimuli. Logvinenko's atlas has several interesting features, which include illumination invariance, reasonable correlation of its coordinate axes with perceptual dimensions, and the possibility of predicting the effects of a change in illuminant colour based on its rectangular metamer reflectances. In this chapter, we aim to evaluate the usefulness of the Gaussian representation of Logvinenko's colour atlas in predicting the change of colour stimuli with the change of illuminant.

2.2 Gaussian-Metamer-Based Prediction of Colour Stimulus Change under Illuminant Change

Perhaps the most common approach to predicting the new LMS under a second illuminant is the von Kries transformation [13] in which each cone channel is independently scaled by a factor proportional to the change in the LMS of a white surface under the second illuminant. For colour stimulus prediction, however, we make use of

Logvinenko's colour atlas. We employ KSM coordinates for predicting illuminant-induced colour stimulus changes, because these coordinates in the atlas specify reflectances; and, as such, they can be computationally 'relit' using the spectrum of the second illuminant to predict what LMS will arise under it. A significant advantage of predicting the colour changes is that the result is guaranteed to be in the metamer set of the actual object surface colour. As Logvinenko points out, for the von Kries method, there is no such guarantee; so that, at least in principle, the von Kries error can be arbitrarily large. In practice, however, using rectangular metamers for the prediction [8] does not always produce the best results on average. The likely reason for this concerns the sharp edges in the rectangular functions. As discussed in Chapter 1, Logvinenko also has proposed [7] a Gaussian parameterization of his colour atlas. Since the Gaussians are smooth by definition, we experiment with them as a vehicle for predicting the effect of illuminant change. This involves first calculating the parameters of the Gaussian metamers.

This involves first calculating the parameters of the Gaussian metamers for which we employ interpolation as discussed in Chapter 1. We also provide a comparison of predicting colour stimulus using the Inverse Gaussians (IG) approach proposed by MacLeod et al.

Note that it is not possible to find IG coordinates for all of the samples. In other words, we cannot come up with a large portion of colours with IG coordinates and we have excluded those samples from this set of experiments to compare KSM, IG and von Kries.

2.3 Results and Discussion

In order to compare using KSM coordinates, IG (inverse Gaussians) coordinates, and the von Kries method of colour stimulus prediction, we first synthesize the LMS tri-stimulus values of Munsell chips [9] under one illuminant (for example D65) using the CIE 1931 colour matching functions [3], and then predict the LMS values under the second illuminant using KSM coordinates, IG coordinates and von Kries scaling [13]. These predictions are compared to the computed ground-truth values (i.e., actual Munsell chip reflectance spectra multiplied by the illuminant spectrum) for the second illuminant. The results for illuminants D65, A, and F11 are tabulated in Table 2.1, and Table 2.2, showing clearly that colour stimulus prediction using KSM coordinates is significantly better in terms of the angular (similar to equation 6 in Chapter 1) and CIEDE2000 error measures than using von Kries scaling. It is also revealed that KSM outperforms IG in almost all the cases.

Table 2.1 Comparison of colour stimulus prediction accuracy for 1400 Munsells using KSM coordinates, Inverse Gaussians (IG), von Kries scaling in terms of the angular error measures calculated similar to equation 6 in Chapter 1 (in degrees).

To	Method	Median	Maximum	Mean
A	KSM	**0.2553**	2.4525	**0.3837**
	IG	0.3354	**2.3963**	0.4755
	von Kries	0.8405	5.2859	1.0897
F11	KSM	**0.3412**	**2.1802**	**0.5793**
	IG	0.3789	4.8939	0.7506
	von Kries	0.6406	6.1444	0.8733

Table 2.2 Comparison of colour stimulus prediction accuracy for 1400 Munsells using KSM coordinates, Inverse Gaussians (IG), and von Kries scaling in terms of the CIEDE2000.

To	Method	Median	Maximum	Mean
A	KSM	**1.0160**	**4.5904**	**1.2676**
	IG	1.2460	5.0165	1.4431
	von Kries	3.7881	10.0098	3.9020
F11	KSM	**1.4337**	**7.4937**	**1.8034**
	IG	1.5946	8.2147	2.2353
	von Kries	2.3621	11.6974	2.7122

Although the lower average prediction errors obtained via the KSM coordinates, as shown in Table 2.1, and Table 2.2, are one advantage of using them, a second important advantage is that the KSM predictions are guaranteed to be in the metamer set, while von Kries predictions are not. In other words, since KSM coordinates by definition specify a reflectance that is metameric to the reflectance generating a given LMS, that KSM reflectance, when relit, must be in the metamer set under the second illuminant. In contrast, von Kries scaling can lead to predicted colour stimuli that fall outside the metamer set. As an example of the type of large errors this can lead to in the case of von Kries, consider the illuminant and reflectance spectra shown in Figure 2.1. Under the second illuminant the actual LMS is (5.0, 5.6, 27) while the von Kries predicts (18, 18, 10) and KSM predicts (8.1, 8.0, 25), with corresponding angular errors of 53 and 8.4 degrees, respectively. Measured in terms of CIEDE2000 these errors are 58.94 and 10 .74 ΔE.

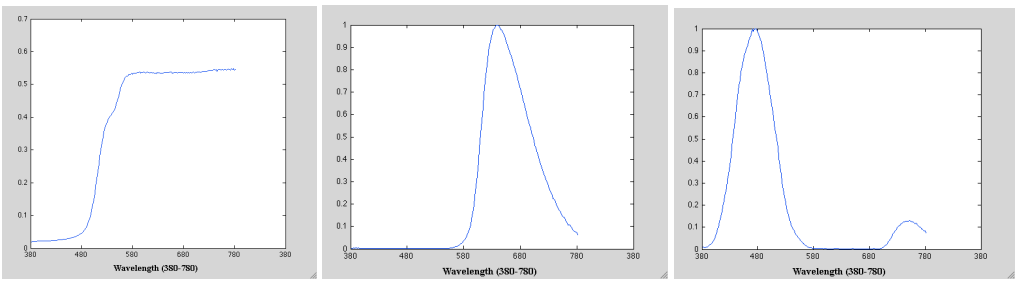

Figure 2.1 Reflectance and illuminant pair for which von Kries fails. Left panel, reflectance; center and right, illuminants.

As another test of KSM coordinates for predicting the colour stimulus under a change of illuminant, we computed the KSM coordinates from the image of the Fruit scene (from [9]) under D65 (see Figure 2.2) and predicted what its image would be under illuminants A and F11. We have also compared the KSM with von Kries for the same prediction procedure. The corresponding results are shown in Figure 2.3, Figure 2.4, and Figure 2.5. Overall, the benefits of KSM over von Kries can be seen once again.

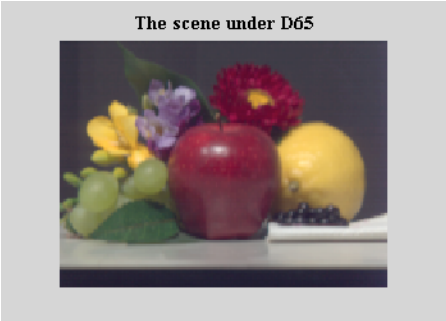

Figure 2.2 Image of the Fruit scene (from [9]) under D65.

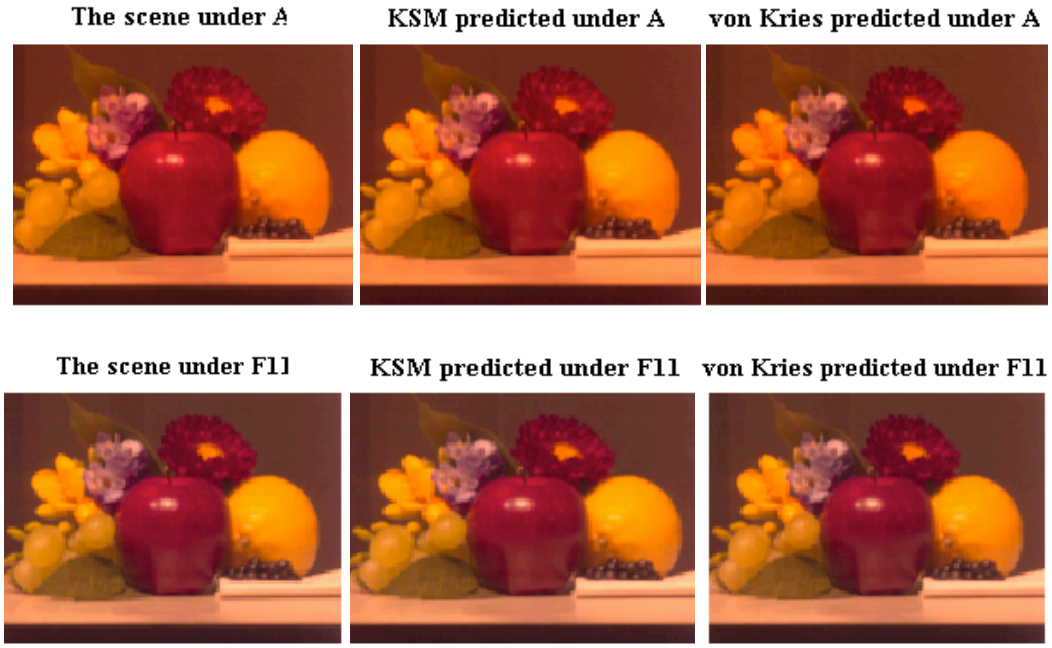

Figure 2.3 **Given the image of the scene under D65 as input, the above images are those predicted by KSM and von Kries for the scene under illuminants A and F11 (correlated colour temperatures 2856K and 4000K). Left-hand column: computed ground-truth image of scene under A (top) and F11 (bottom). Middle column: images predicted by KSM for scene under A and F11. Right-hand column: images predicted by von Kries for A and F11.**

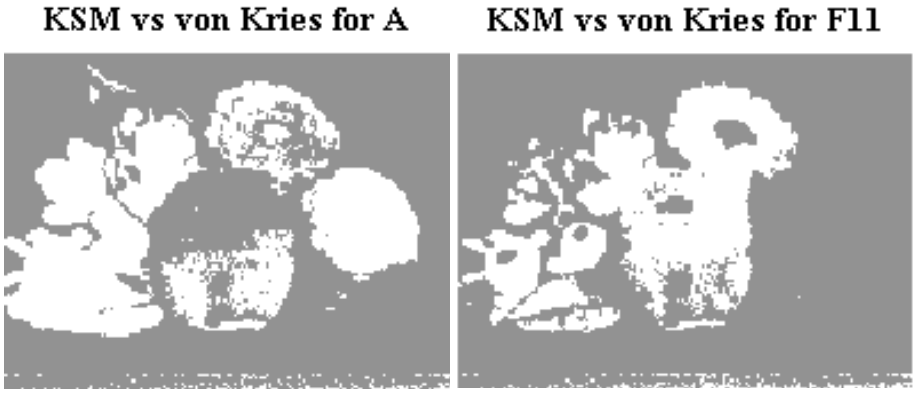

Figure 2.4 **Comparison of KSM and von Kries using maps of the difference in pixel-by-pixel angular error for the predicted images shown in Figure 2.3. White indicates that the KSM error is at least 0.5 degrees less than von Kries; grey indicates the absolute error difference between them is less than 0.5 degrees; black indicates a von Kries error at least 0.5 degrees less than that of KSM.**

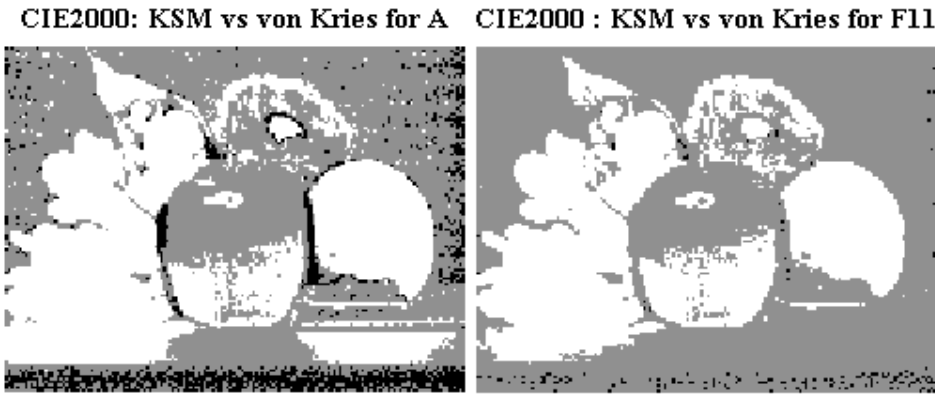

Figure 2.5 Comparison of KSM and von Kries using maps of the difference in CIEDE2000 error for the predicted images shown in Figure 2.3. White indicates that the KSM error is at least 0.5 delta E less than von Kries; grey indicates the absolute error difference between them is less than 0.5 delta E; black indicates a von Kries error at least 0.5 delta E less than that of KSM.

In order to further explore the usefulness of KSM coordinates in colour stimulus prediction, we have done the same prediction procedure for the 6 special illuminants introduced by Logvinenko and 1995 Munsell samples found in [9]. The results in terms of median, maximum, and average of angular errors are tabulated in Table 2.3. The results of the same procedure, measured in terms of CIEDE 2000, are shown in Table 2.4.

In addition, considering all the experiments together, the median, maximum, and average error rates are revealed in Table 2.5 and Table 2.6.

As it can be seen in Table 2.3 and Table 2.4, although in a few cases KSM has a larger error, it generally reveals superior results over von Kries in both angular and CIEDE2000 measures. Being interested in a single summary statistic able to compare the whole set of error measures, the experimental results are also evaluated using the Wilcoxon Sign Test [11]. The Wilcoxon Sign Test confirms the superiority of KSM over von Kries in terms of angular and CIEDE2000 error measures with a confidence of 95%.

Looking carefully at the illuminant spectra, we note that they have portions with very small values, essentially violating a basic requirement of Logvinenko's colour atlas theory, which is that the illuminants be strictly positive. Note that these illuminants are not typical types of illuminants. They were suggested by Logvinenko for his psychophysical experiments. The near-zero values in the illuminants can sometimes lead to large errors in the colour stimulus prediction.

As an example of the type of large errors for KSM, consider the illuminant and reflectance spectra shown in Figure 2.6. Under the second illuminant the actual LMS is (14.5,4.6,3.3607) while KSM predicts (0.6,0.8,7.4). This is because the Gaussian metamer fails to capture the non-zero part of the reflectance that falls under the second illuminant ($580 \leq \lambda \leq 680$) since the first illuminant is almost zero in this range.

In order to fulfil Logvinenko's conditions, the illuminants should be strictly positive everywhere. We have performed another set of experiments employing a set of illuminants produced by adding an offset (10 percent of the peak value) to each of the original ones. This way we avoid the problems associated with the illuminants with near-zero values we had before.

The results in terms of angular error and CIEDE2000 for different cases are reported in Table 2.7 and Table 2.8, respectively. In addition, summaries of the corresponding error rates for the whole samples are tabulated in Table 2.9 and Table 2.10. As it can be in clearly inferred from the tables, KSM colour stimulus prediction significantly outperforms von Kries in median, maximum and average errors in both angular and CIEDE2000 measures.

Table 2.3 Comparison of prediction angular error rates for Munsell chips found in [9].

Illuminant Number		Median		Max		Mean	
From	**To**	**KSM**	**von Kries**	**KSM**	**von Kries**	**KSM**	**von Kries**
1	**2**	**1.74**	2.73	31.03	**26.35**	**3.71**	4.04
1	**3**	**2.09**	3.15	**22.30**	23.39	**2.74**	3.81
1	**4**	**1.70**	2.61	**19.76**	20.07	**2.37**	3.42
1	**5**	1.24	**1.16**	55.73	**29.17**	3.67	**1.80**
1	**6**	0.80	**0.47**	32.57	**9.61**	2.03	**0.66**
2	**1**	**0.22**	0.63	**5.40**	7.53	**0.39**	0.82
2	**3**	**1.76**	3.80	30.17	**27.85**	**2.57**	5.14
2	**4**	**1.75**	3.12	**28.16**	31.23	**2.62**	4.44
2	**5**	**1.07**	1.50	70.96	**30.79**	3.38	**2.25**
2	**6**	0.70	**0.54**	69.75	**9.70**	1.79	**0.80**
3	**1**	**0.30**	1.85	**6.63**	23.74	**0.48**	2.69
3	**2**	**1.08**	4.83	**22.87**	46.04	**1.85**	6.48
3	**4**	**0.14**	0.49	**2.91**	7.53	**0.23**	0.69
3	**5**	**0.57**	1.21	29.53	**25.41**	**1.16**	1.78
3	**6**	**0.48**	0.89	11.54	**7.47**	**0.87**	1.18
4	**1**	**0.30**	1.82	**7.28**	22.97	**0.50**	2.74
4	**2**	**1.36**	5.57	**24.10**	46.95	**2.28**	7.40
4	**3**	**0.17**	0.64	**2.95**	6.62	**0.28**	0.90
4	**5**	**0.58**	1.01	**21.18**	23.22	**1.07**	1.58
4	**6**	**0.48**	0.81	10.35	**6.93**	**0.82**	1.11
5	**1**	**0.52**	1.40	**13.23**	25.02	**0.81**	2.12
5	**2**	**2.74**	9.85	**22.62**	53.60	**3.97**	12.10
5	**3**	**1.87**	3.42	**17.37**	34.91	**2.45**	5.08
5	**4**	**1.44**	2.25	**15.23**	34.31	**1.91**	3.46
5	**6**	**0.07**	0.11	**1.63**	2.40	**0.12**	0.16
6	**1**	**0.50**	1.54	**10.75**	28.44	**0.76**	2.28
6	**2**	**2.80**	10.17	**53.76**	55.95	**4.29**	12.60
6	**3**	**1.82**	3.88	**21.40**	37.89	**2.48**	5.80
6	**4**	**1.43**	2.59	**16.86**	38.30	**1.92**	4.01
6	**5**	**0.13**	0.21	**5.93**	6.00	**0.24**	0.37

Table 2.4 Comparison of prediction CIEDE2000 error rates for Munsell chips found in [9].

Illuminant Number		Median		Max		Mean	
From	**To**	**KSM**	**von Kries**	**KSM**	**von Kries**	**KSM**	**von Kries**
1	**2**	**1.88**	5.20	**18.88**	26.73	**3.20**	6.44
1	**3**	7.51	**6.90**	**23.67**	26.27	8.19	**7.99**
1	**4**	9.52	**7.18**	**26.73**	27.48	9.91	**8.33**
1	**5**	24.66	**9.85**	**50.93**	56.03	23.96	**12.64**
1	**6**	26.40	**10.34**	**58.37**	60.08	25.76	**13.40**
2	**1**	**1.56**	5.21	**11.26**	26.73	**2.11**	6.45
2	**3**	**5.62**	9.71	39.56	**31.48**	**7.10**	10.98
2	**4**	**6.89**	10.80	41.80	**35.47**	**8.32**	12.06
2	**5**	17.36	**13.40**	72.41	**63.05**	18.46	**16.38**
2	**6**	19.19	**14.27**	76.10	**67.17**	20.19	**17.36**
3	**1**	**1.95**	6.90	**13.89**	26.27	**2.72**	7.99
3	**2**	**1.89**	9.71	**18.54**	31.48	**2.83**	10.98
3	**4**	**0.54**	1.69	**3.31**	5.92	**0.70**	1.83
3	**5**	**4.72**	9.04	**18.57**	52.80	**5.09**	11.93
3	**6**	**4.74**	10.39	**21.72**	59.36	**5.40**	13.43
4	**1**	**2.03**	7.19	**13.54**	27.48	**2.80**	8.33
4	**2**	**2.49**	10.80	**20.18**	35.47	**3.52**	12.06
4	**3**	**0.58**	1.69	**3.26**	5.92	**0.74**	1.83
4	**5**	**4.28**	7.88	**16.53**	48.74	**4.66**	10.56
4	**6**	**4.23**	9.11	**18.68**	55.23	**4.81**	12.02
5	**1**	**5.92**	9.85	**28.43**	56.03	**7.01**	12.64
5	**2**	**7.06**	13.39	**34.85**	63.05	**8.35**	16.38
5	**3**	**4.74**	9.03	**24.81**	52.80	**5.75**	11.93
5	**4**	**4.71**	7.87	**24.55**	48.74	**5.59**	10.55
5	**6**	**1.10**	1.46	**7.33**	11.25	**1.23**	2.00
6	**1**	**5.17**	10.34	**25.99**	60.08	**6.15**	13.40
6	**2**	**6.08**	14.25	**30.05**	67.17	**7.35**	17.35
6	**3**	**4.75**	10.39	**22.84**	59.36	**5.78**	13.42
6	**4**	**5.00**	9.10	**23.10**	55.23	**5.90**	12.02
6	**5**	**1.03**	1.46	**8.30**	11.25	**1.20**	2.00

Table 2.5 Overall comparison of prediction angular error rates for Munsell chips found in [9].

Median		Max		Mean	
KSM	**von Kries**	**KSM**	**von Kries**	**KSM**	**von Kries**
0.7531	1.5470	70.9598	55.9529	1.7928	3.3910

Table 2.6 Overall comparison of prediction CIEDE2000 error rates for Munsell chips found in [9].

Median		Max		Mean	
KSM	**von Kries**	**KSM**	**von Kries**	**KSM**	**von Kries**
4.7583	8.0223	76.1024	67.1741	7.1599	10.4897

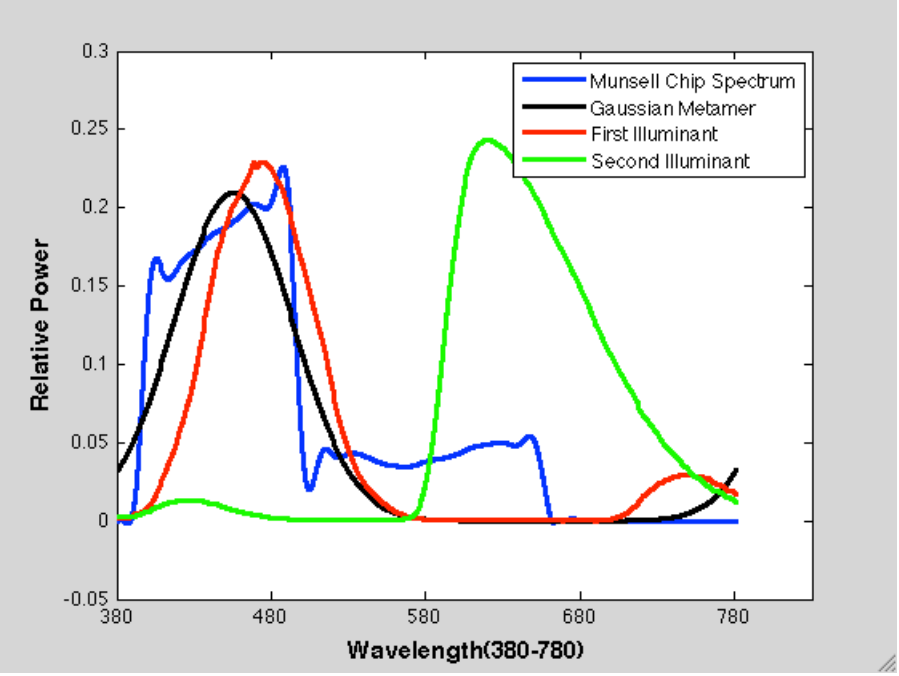

Figure 2.6 **Reflectance and illuminant pair for which KSM fails. Blue curve: reflectance; Black curve: the Gaussian metamer; Red and Green curves: First and Second illuminants. Note that the illuminants are scaled. The Gaussian metamer fails to capture the non-zero part of the reflectance that falls under the second illuminant in the range $580 \leq \lambda \leq 680$.**

Table 2.7 Comparison of prediction angular error rates for Munsell chips found in [9] when adding an offset to the illuminants.

Illuminant Number		Median		Max		Mean	
From	**To**	**KSM**	**von Kries**	**KSM**	**von Kries**	**KSM**	**von Kries**
1	**2**	**1.09**	2.09	**7.64**	11.97	**1.56**	2.67
1	**3**	**0.65**	1.65	**5.58**	11.07	**0.86**	2.19
1	**4**	**0.57**	1.59	**5.52**	12.95	**0.86**	2.25
1	**5**	**1.05**	2.01	**23.59**	28.76	**2.17**	3.15
1	**6**	**1.14**	2.31	**22.38**	26.24	**2.33**	3.46
2	**1**	**0.35**	1.12	22.14	**14.47**	**0.58**	1.60
2	**3**	**0.54**	2.12	**7.70**	20.26	**0.83**	2.80
2	**4**	**0.58**	2.07	**10.53**	25.37	**0.95**	2.77
2	**5**	**0.90**	2.41	**15.44**	33.03	**1.57**	3.62
2	**6**	**1.04**	2.47	**14.78**	31.74	**1.78**	3.75
3	**1**	**0.24**	1.34	**5.41**	9.63	**0.38**	1.83
3	**2**	**0.76**	3.13	**6.71**	13.01	**1.10**	3.73
3	**4**	**0.13**	0.45	**2.48**	6.52	**0.21**	0.64
3	**5**	**0.63**	1.24	**10.82**	20.57	**1.05**	2.01
3	**6**	**0.66**	1.29	**11.76**	17.75	**1.20**	2.09
4	**1**	**0.25**	1.39	**7.13**	10.41	**0.43**	1.96
4	**2**	**1.02**	3.87	**8.03**	16.18	**1.42**	4.64
4	**3**	**0.16**	0.56	**2.44**	5.74	**0.25**	0.80
4	**5**	**0.59**	0.94	**8.49**	16.05	**0.95**	1.55
4	**6**	**0.61**	0.99	**10.52**	14.02	**1.09**	1.70
5	**1**	**0.54**	1.92	**17.17**	20.17	**0.88**	2.92
5	**2**	**1.41**	6.47	**11.78**	28.86	**1.85**	7.58
5	**3**	**0.87**	2.13	**7.47**	18.62	**1.11**	3.06
5	**4**	**0.64**	1.20	**8.31**	14.36	**0.89**	1.84
5	**6**	**0.18**	0.58	**3.75**	4.11	**0.31**	0.75
6	**1**	**0.50**	2.54	**12.33**	18.52	**0.76**	3.54
6	**2**	**1.14**	6.22	**10.19**	28.21	**1.53**	7.25
6	**3**	**0.70**	2.11	**5.95**	15.24	**0.88**	2.98
6	**4**	**0.56**	1.23	**5.77**	13.59	**0.79**	1.98
6	**5**	**0.17**	0.58	4.31	**4.11**	**0.32**	0.75

Table 2.8 Comparison of prediction CIEDE2000 error rates for Munsell chips found in [9] when adding an offset to the illuminants.

Illuminant Number		Median		Max		Mean	
From	**To**	**KSM**	**von Kries**	**KSM**	**von Kries**	**KSM**	**von Kries**
1	**2**	**1.94**	4.77	**9.40**	21.56	**2.40**	5.44
1	**3**	**2.08**	4.34	**7.97**	14.03	**2.26**	4.98
1	**4**	**2.34**	4.37	**9.75**	16.63	**2.59**	5.34
1	**5**	**7.27**	7.01	**22.76**	38.24	**7.45**	9.07
1	**6**	**7.66**	7.89	**26.31**	34.56	**7.95**	9.54
2	**1**	**2.52**	4.77	**11.73**	21.56	**2.99**	5.44
2	**3**	**1.73**	5.31	**9.64**	20.31	**2.30**	5.78
2	**4**	**2.10**	6.67	**12.70**	25.74	**2.81**	7.25
2	**5**	**4.61**	10.04	**23.14**	42.41	**5.02**	11.32
2	**6**	**5.12**	10.26	**27.84**	36.09	**5.71**	11.08
3	**1**	**0.99**	4.34	**5.83**	14.03	**1.21**	4.98
3	**2**	**1.64**	5.31	**9.37**	20.31	**2.20**	5.78
3	**4**	**0.48**	1.50	**3.07**	5.32	**0.62**	1.62
3	**5**	**3.19**	4.85	**14.57**	30.29	**3.39**	6.19
3	**6**	**3.22**	4.63	**18.03**	25.58	**3.61**	5.80
4	**1**	**1.11**	4.37	**7.05**	16.63	**1.48**	5.34
4	**2**	**2.20**	6.67	**11.88**	25.74	**2.86**	7.25
4	**3**	**0.52**	1.50	**3.06**	5.32	**0.66**	1.62
4	**5**	**2.74**	3.43	**11.45**	27.70	**2.93**	4.77
4	**6**	**2.74**	3.53	**14.41**	23.02	**3.05**	4.66
5	**1**	**2.38**	7.01	**16.52**	38.24	**2.93**	9.07
5	**2**	**3.14**	10.03	**18.00**	42.41	**3.84**	11.31
5	**3**	**2.07**	4.85	**10.39**	30.29	**2.38**	6.19
5	**4**	**2.24**	3.43	**8.71**	27.70	**2.49**	4.77
5	**6**	**0.66**	2.26	**2.67**	9.38	**0.73**	2.50
6	**1**	**2.04**	7.89	**12.98**	34.56	**2.47**	9.55
6	**2**	**2.67**	10.27	**16.33**	36.09	**3.35**	11.09
6	**3**	**1.92**	4.63	**10.06**	25.58	**2.24**	5.80
6	**4**	**2.23**	3.54	**8.62**	23.02	**2.45**	4.66
6	**5**	**0.64**	2.26	**2.85**	9.38	**0.72**	2.50

Table 2.9 Overall comparison of prediction angular error rates for Munsell chips found in [9] when adding an offset to the illuminants.

Median		Max		Mean	
KSM	**von Kries**	**KSM**	**von Kries**	**KSM**	**von Kries**
0.5675	1.6289	23.5916	33.0323	1.0298	2.7283

Table 2.10 Overall comparison of prediction CIEDE2000 error rates over all samples for Munsell chips found in [9] when adding an offset to the illuminants.

Median		Max		Mean	
KSM	**von Kries**	**KSM**	**von Kries**	**KSM**	**von Kries**
2.2972	4.7782	27.8382	42.4058	2.9031	6.3561

2.4 Summary

Colour stimulus prediction plays an important role in many colour-related applications. In this chapter we investigated the usefulness of Gaussian metamer parameterization of Logvinenko's rectangular metamer colour atlas (KSM) in colour stimulus prediction with the change of illuminant. We showed experimentally that the KSM coordinates are helpful for predicting the change in colour stimulus that arises under a change of illumination or observer sensitivity functions. As we might expect based on the invariance property of KSM colour coordinates, in addition to providing better predictions on average, employing them for colour stimulus prediction has the advantage over von Kries scaling in that it is guaranteed to provide answers that lie within the metamer set of the original colour stimulus. We also performed a set of experiments showing the advantage of KSM over inverse Gaussians in both calculating the colour coordinates and colour stimulus prediction.

3: COLOUR CONSTANCY: INTERSECTING COLOUR MANIFOLDS

3.1 Introduction

Colour constancy has been defined as finding colour descriptors that are invariant to illumination changes [14]. This domain has proven to be useful for accurate and constant colours in digital cameras, printers and displays. In addition, the illuminant independent colour descriptors calculated after the estimation of the light, can be used in a variety of computer vision applications.

Many strategies have been proposed to address colour constancy. Many methods aim to retrieve the chromaticity of the illumination, and ignore its intensity [15] [16][17][18][19][20]. If we use the angular difference measure between the colour vectors we are indeed dealing with chromaticity. There are some advantages for this including more robustness to intensity variations, as well as the reduction of computational complexity. Most importantly, the exposure information for most images is unknown, therefore there is no way to solve for the illumination intensity.

The simplest approach for colour constancy is perhaps to assume uniform illumination for the whole scene and characterize this illumination with a simple statistic. Perhaps the best-known colour constancy algorithm, gray world [21], uses the mean operation and assumes that the average of all the reflectances must be gray. One challenge may be specifying the gray colour. In addition, it is obvious that the assumption does not always hold.

The next family of constancy techniques are called Gamut-Mapping methods. The basic idea is to compute a mapping between colour gamuts (i.e., the complete range of colour signals obtainable for given sensors under a given light) calculated under the canonical light and unknown illuminants. This mapping is a transform of the colour-space coordinates of the elements of a source image to colour-space coordinates of the elements of a target image. The first stage is to find the map between canonical gamut i.e., the set of all possible sensor responses under the canonical light and the image gamut [16][17][22][23][24][25][26]. There are many feasible mappings for an image. In order to estimate the illuminant one should find the best map as the solution. One way to do so is to use the average of all the possible maps or select the mapping, which maximizes the volume of the mapped set. Some of the gamut-mapping methods disregard intensity information and therefore project the gamuts into a 2D chromaticity space, which has the advantages mentioned before.

There are some colour constancy approaches that assume a priori information about the distribution of lights and surfaces in the world. Using the Bayesian rule, therefore, and given a set of observed colours, one can find the posterior probabilities of the illuminants and surfaces in a scene. The general idea is to determine the likelihood of a set of solutions instead of a unique answer. The colour by correlation [20] approach falls into this category and basically employs a direct Bayes rule in the illumination estimation problem. In this approach, the probability of observing each particular chromaticity under each illuminant is computed and, thereby, given the chromaticities of the entire scene, the likelihood of each illuminant is computed. Eventually, one can chose the most likely illuminant. There are also some neural network based methodologies for

the colour constancy problem reported in the past few years [19][27][28]. The neural network is trained using a lot of images. The features can be defined as the chromaticities occurring under each illuminant. This network can be later used to estimate the illuminant for a given image. Of course different colour constancy approaches can be combined to gain a better estimate of the true light [29].

Colour constancy, because of its importance in a lot of computer vision applications, has gained much attention and still remains a challenging problem due to the fact that it is so under-constrained. We approach the colour constancy problem from the KSM perspective by estimating the illuminant chromaticity based on decomposition of a colour tri-stimulus values into illuminant and reflectance Gaussian functions.

Logvinenko's colour atlas [1] provides a way to enumerate a complete and unique set of colour-equivalent stimuli (material reflectance and illuminant spectral pairs that have the same appearance) for all possible RGB tri-stimulus values [7]. In his theory, both the material reflectance and illuminant spectra are each specified by 3 parameters, so a colour-equivalent stimulus is specified by 6 parameters. For a given tri-stimulus value, the set of colour-equivalent stimuli defines a 3-dimensional manifold, which he terms the material-lighting-invariance manifold. Using this theoretical structure, we propose a new illumination-estimation method. For an image of a scene under a single illuminant, two different RGBs, from two different pixels, define two different material-lighting-invariance manifolds. Since by assumption they share a common illuminant, that illuminant must lie within the intersection of those two manifolds. However, the intersection is not, in general, a single value, but rather a set of values. Intersecting the manifolds defined by the RGBs from other pixels further constrains the range of possible

scene illuminants. Tests with real images show that the method's performance is comparable to that of other well-known methods. An advantage of the proposed method is that it is founded on the theoretical principles of the colour atlas and exploits precisely the theoretical constraints the atlas provides.

Many strategies have been proposed for estimating the chromaticity of the scene illumination. The present approach has some similarities to Forsyth's gamut mapping method [22] and the voting methods (Colour by Correlation [30] and Sapiro's Illuminant Voting [31]). It relates to gamut mapping in that it represents a set of constraints and derives information from their intersection. It relates to Colour by Correlation and Illuminant Voting in that the intersection of the manifold is implemented via voting for candidate illuminants.

3.2 Background

The camera or eye's response to light with the spectral power distribution $E(\lambda)$ of light reflected from a matte, non-specular surface material with reflectance $S(\lambda)$ is modelled in the standard way as the triplet φ_i (i=1,2,3):

$$\varphi_i = \int_{\lambda_{\min}}^{\lambda_{\max}} E(\lambda)S(\lambda)R_i(\lambda)d\lambda \qquad i = 1,2,3 \qquad (1)$$

where $R_i(\lambda)$ is the spectral sensitivity function of the sensor.

Logvinenko [7] defines a light-colour atlas A_p as a subset of light spectral functions (strictly positive ones) such that given any colour stimulus (object material reflectance x illuminated by light spectrum p) there is a unique element in the light-colour

atlas such that, illuminating x, this element results in a metameric match to the given colour stimulus. There is a similar definition for the object-colour atlas A_x. An object-colour atlas is defined as a set of object material functions A_x such that for each colour stimulus there is a unique element in A_x such that, if illuminated by p, this element results in a metameric match to the given colour stimulus.

Logvinenko further defines a general colour atlas in terms of an object-colour atlas A_x and a light-colour atlas A_p. The colour atlas A is such that for any object illuminated by any light, there is a unique element p from A_p and a unique element x from A_x that is colour equivalent to the input pair. Colour equivalence means being indistinguishable in colour appearance; however, in the special case of single-illuminant scenes it corresponds to metamerism [7]. For an arbitrary colour stimulus (x',p') therefore there is a unique pair (x,p) in the colour atlas that is colour equivalent to it. By virtue of the definition of a colour atlas, there will be a one-to-one map between any two atlases. The set of all colour-equivalent object/light pairs is called the object-colour set. Logvinenko refers to the object-colour set along with the set of coordinates systems defined by the family of colour atlases as the object-colour manifold.

For any given colour stimulus (x,p) its coordinates in the general colour atlas can be determined by 2-step colour matching [7]. Step 1 is to find the unique element a_m from the object-colour atlas such that

$$\varphi_i(x,p)=\varphi_i(a_m,p) \qquad i=1,2,3 \qquad (2)$$

Step 2 is then to find the unique element a_l from the light-colour atlas such that

$\varphi_i(a_m,p)=\varphi_i(a_m,a_l)$ $\quad i=1,2,3$ (3)

Since the object-colour atlas and the light-colour atlas are each 3-dimensional, the resulting coordinates of the general colour atlas are 6-dimensional.

The object reflectances and light spectra of the colour atlases can be represented in terms of rectangular functions [1] that are a mixture of uniform gray and a rectangular component that takes only values 0 and 1, with at most 2 transitions between 0 and 1. These rectangular functions are very unlike typical reflectance and illuminant spectral functions and hence are not very suitable for our purposes. However, Logvinenko also proposes other parameterizations of the colour atlas, one of which is based on a Gaussian representation of spectra. The Gaussian representation is given in terms of a 3-parameter set of spectral reflectance functions $g_m(\lambda;k_m,\sigma_m,\mu_m)$ and a similar 3-parameter set of spectral power distribution functions $g_l(\lambda;k_l,\sigma_l,\mu_l)$, both of which are Gaussian-like (see equations 1-4 of chapter 1) functions, where k, σ, and μ indicate the height, standard deviation and center (peak) of the Gaussian. The functions are not strictly Gaussians in that they wraparound from one end of the visual spectrum to the other. They also differ from the inverse Gaussians used by Macleod et al. [5].

Any given sensor response triplet φ_i (i =1,2,3) can be decomposed into a sextuplet $(k_m,\sigma_m,\mu_m,k_l,\sigma_l,\mu_l)$ representing a Gaussian-like material reflectance lit by a Gaussian-like illuminant such that

$$\int_{\lambda_{min}}^{\lambda_{max}} g_l(\lambda;k,\sigma_l,\mu_l)g_m(\lambda;k,\sigma_m,\mu_m)R_i(\lambda)d\lambda = \varphi_i \qquad i=1,2,3 \qquad (4)$$

This decomposition is not unique; however, each choice of illuminant uniquely defines a corresponding material and vice-versa. For a given sensor response triplet, the set of all such illuminant-material pairs defines a 3-dimensional manifold embedded in a 6-dimensional space.

Illumination-estimation generally means estimating only the chromaticity of the illuminant, since for colour balancing the intensity of the illuminant does not matter. In the present case, disregarding the intensity of the illumination or any uniform scaling of the percent surface spectral reflectance function reduces the number of parameters from six to four $(\sigma_m,\mu_m,\sigma_l,\mu_l)$. Defining chromaticity in the standard way as $\tau_i = \varphi_i/(\varphi_1 + \varphi_2 + \varphi_3)$ (i=1,2) then similar to (4), any sensor chromaticity can be decomposed as

$$\int_{\lambda_{min}}^{\lambda_{max}} g_l(\lambda;1,\sigma_l,\mu_l)\, g_m(\lambda;1,\sigma_m,\mu_m) R_i(\lambda) d\lambda = n\tau_i \qquad i = 1,2 \tag{5}$$

where n is an arbitrary multiplier. The resulting parameters lie on a 2-dimensional manifold embedded in a 4-dimensional space. Figure 3.1 shows two examples of the manifolds defined by different input sensor chromaticity values.

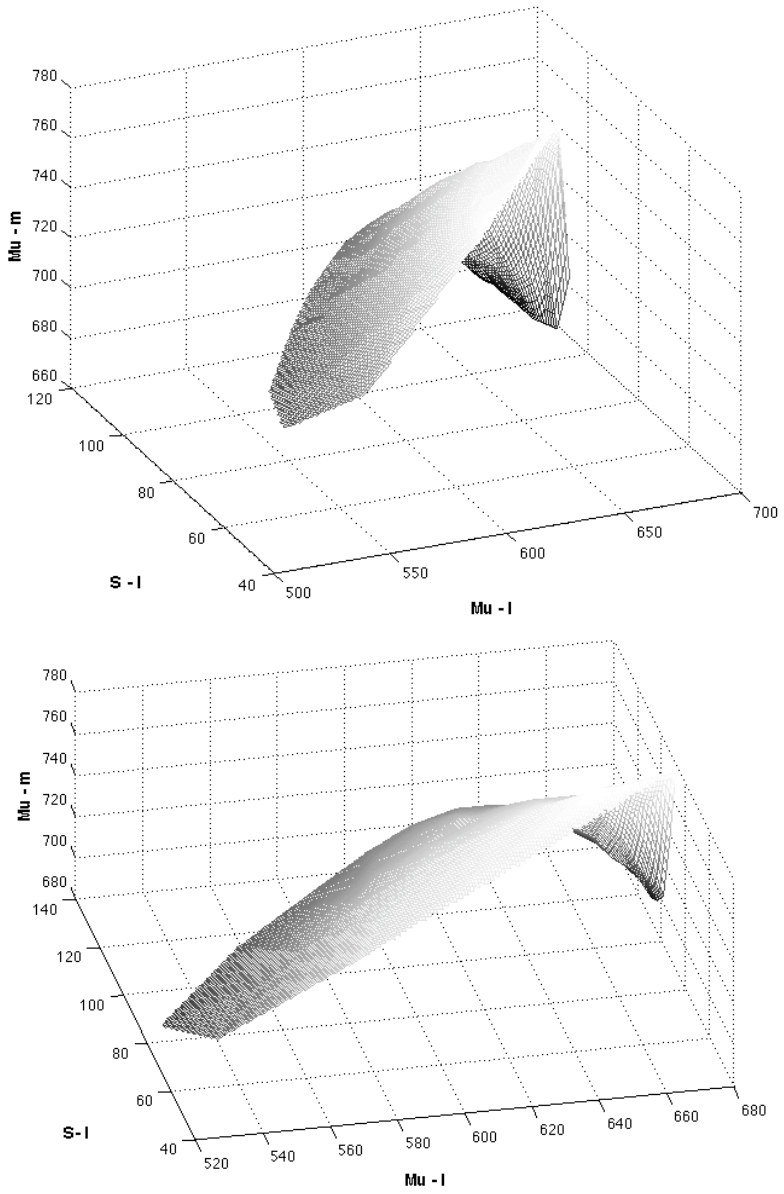

Figure 3.1 Plots of the 2-dimensional material-illuminant manifold embedded in the 4-dimensional space of $\mu_l,\sigma_l,\mu_m,\sigma_m$ for two different input chromaticity values. Axes are Mu-l, Mu-m, S-l, S-m for $\mu_l,\sigma_l,\mu_m,\sigma_m$ respectively. Three of the dimensions (i.e., μ_l,σ_l,μ_m) are represented by the axes. Note that the fourth dimension σ_m is not represented. Top and bottom panels illustrate the manifold for chromaticity values of (.53 .13) and (.66 .13) based on the SONY DXC-930 sensor sensitivity functions, respectively.

3.3 Proposed Manifold Intersection Method

Given an RGB image of a single-illuminant scene, each distinct RGB value implies a manifold of illuminant-material pairs. Two different RGBs taken from the same single-illuminant image will define two different manifolds. For each RGB the set of possible illuminants consistent with it is represented by the illuminant components of the 4D manifold, so projection of the manifold onto the illumination axes results in the possible illuminants consistent with the given RGB. The illuminants consistent with two RGBs lie in the intersection of their projections. Each additional RGB will further limit the common intersection. To determine the overall scene illuminant, every distinct RGB from the image is used to limit the set of potential illuminant candidates as much as possible.

To compute the intersections, we use a Hough-transform-like approach. At first it might seem that the $(\sigma_m,\mu_m,\sigma_l,\mu_l)$ space would require a 4-dimensional Hough accumulator array, however, since we are only interested in the illuminant a 2-dimensional array will suffice. The illuminant space is discretized and a 2-dimensional accumulator array is used. Given an image RGB, each $(\sigma_m,\mu_m,\sigma_l,\mu_l)$ point on the manifold defined by it increments the corresponding accumulator array cell (σ_l,μ_l) by a single vote. Once all the image's distinct RGBs have been processed, the accumulator array cell with the most votes determines the scene illuminant. If there is not a unique maximum, the illuminant estimates are averaged.

3.3.1 Implementation Details

The advantage of the light-colour and object-colour atlases is that they provide a means by which we can enumerate a unique set of illuminant and material spectra that completely covers the entire colour space without any redundancy. In particular, we can enumerate the complete set of Gaussian illuminants from the light-colour atlas by stepping through values of μ_l and σ_l, and are guaranteed that each will be of a different chromaticity. In practice, a step size must be chosen. Stepping uniformly in each of μ_l and σ_l discretizes the 2D space into bins. Experimentally, the ranges of both μ_l and σ_l were divided into 20 intervals each, for a total of 400 accumulator array bins.

To facilitate the voting procedure, we pre-compute a table containing all the possible material-lighting pairs (σ_l,μ_l) and (σ_m,μ_m) along with the corresponding (τ_1,τ_2) chromaticity values they would produce given sensor sensitivity functions $R_k(\lambda)$ according to Equation 4. The Gaussian illuminant spectrum $g_l(\lambda)$ and the Gaussian reflectance spectrum $g_m(\lambda)$ are both easily computed from the wraparound Gaussian definition of equations 1-4 of Chapter 1. Since only chromaticities are required, we can set both $k_m=1$ and $k_l=1$ and compute the chromaticity of the sensor response using Equation 5.

For the look-up table to be complete, all possible $(\sigma_l,\mu_l),(\sigma_m,\mu_m)$ pairs should be considered, which leads once again to a choice of step-size. Larger steps mean a coarser quantization; smaller steps mean a larger table. In the tests reported below μ and σ are discretized as:

μ: $380 \leq \lambda \leq 780$ in steps of 5nm

$0 \leq \sigma \leq 400$ in steps of 5 nm

This choice of step-size leads to a table of about 10^7 entries, each entry consisting of 6 variables $(\sigma_1,\mu_1,\sigma_2,\mu_2,\tau_1,\tau_2)$..

The voting process for each input chromaticity (τ_1^0,τ_2^0) then involves finding all the table entries of matching chromaticity. Two chromaticities are considered to match when $norm(\tau_1^0-\tau_{table})$ is small.

3.3.2 Algorithm Summary

1. Pre-compute a table consisting of all the pairs of (σ_l,μ_l) and (σ_m,μ_m) along with their corresponding chromaticities at a given quantization step-size.
2. Given an image, compute its chromaticity histogram. The tests below are based on a 30x30 histogram. Binarize the histogram based on a threshold on the minimum number of occurrences. This eliminates spurious chromaticity values created by noise.
3. For every distinct image chromaticity, find all the matching chromaticities in the table and return the corresponding σ_l and μ_l pairs.
4. For each (σ_l,μ_l) pair found in step 3, increment the accumulator array with a vote for that illuminant.
5. Once all distinct image chromaticities have been processed, the scene illuminant is determined by the (σ_l,μ_l) of the accumulator array bin with the maximum number of votes.

Figure 3.2 shows an example of an accumulator array filled with votes. Given (σ_l,μ_l), its

chromaticity is easily computed via Equation 5.

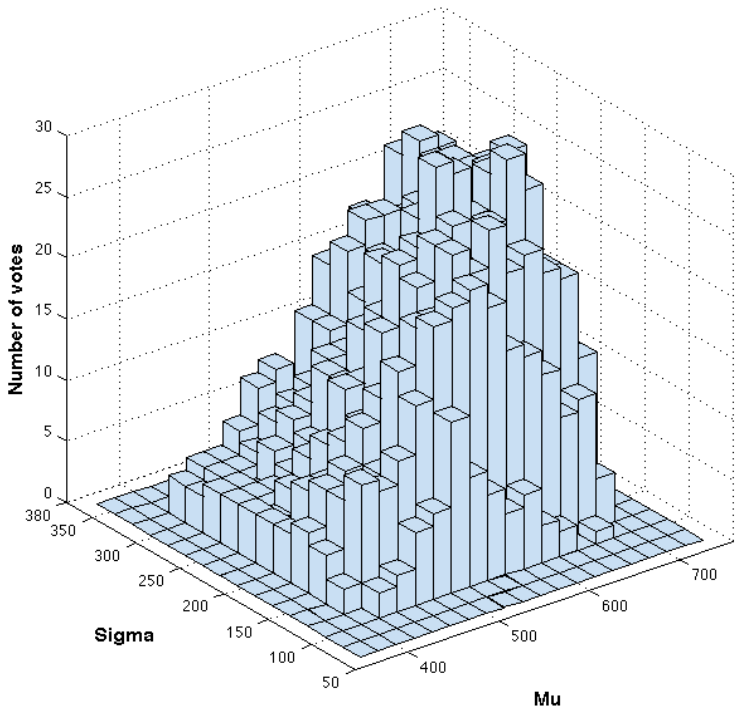

Figure 3.2 An example of the accumulator array of votes generated by 30 image RGBs. The ranges of peak wavelength μ and spectral bandwidth σ, which are [380nm, 780nm] and [0,400] respectively, have been divided into 20 intervals, giving 400 bins in total.

3.4 Results

The Manifold Intersection method has been tested on both the SFU 321-image set [32][33] and the SFU HDR image set [34][35]. These are the only two colour constancy datasets we are aware of that include the spectral sensitivity functions for the cameras used. Its performance is compared to that of MaxRGB algorithm, MaxRGB (bicubic pre-processing version of [35]), Greyworld, Do-Nothing, Greyedge [36][37], and Colour by Correlation Bright (Colour by Correlation using bright pixels only [30] and tested on only 310 of the 321 images). The images in the 321-set are linear (gamma=1) images of indoor

scenes. The results are tabulated in Table 3.1. The Do-Nothing error is the error obtained by simply assuming the scene illumination is always white (i.e., estimating its chromaticity as r=g=b=1/3).

For the HDR set, we computed a second look-up table based on the spectral sensitivity functions for the Nikon D700 camera used for that dataset. Table 3.2 illustrates the performance of the Manifold Intersection method in comparison to the other methods on HDR image dataset.

Table 3.1 Performance of Manifold Intersection in comparison to other well-known illumination-estimation methods on the 321 linear images of the SFU dataset. The error measure is angular error in degrees.

	Median	**Average**	**Max**
Do-Nothing	16	17	37
Grey World	7.1	9.8	7
Max RGB code of [37]	6.5	9.1	36
Grey Edge	3.7	6.1	28
SoG	4.0	6.0	25
MaxRGB (bicubic)	3.1	5.6	27
CbyC bright from Table V of [30]	3.2	6.6	
Manifold Intersection	**4.9**	**6.7**	**29**

Table 3.2 Performance of Manifold Intersection in comparison to other well-known illumination-estimation methods on the 105 linear images of the SFU HDR dataset. The error measure is angular error in degrees.

	Median	**Average**	**Max**
Do-Nothing	15	15	30
Grey world	7.3	7.9	23
Grey Edge	3.9	6.0	25
SoG	4.0	6.0	25
MaxRGB (bicubic)	3.9	6.3	28
Manifold Intersection	**4.4**	**7.1**	**24**

3.5 Summary

Logvinenko's colour atlas theory provides a structure in which a complete set of colour-equivalent material and illumination pairs can be generated to match any given input RGB colour. In chromaticity space, the set of such pairs forms a 2-dimensional manifold embedded in a 4-dimensional space. This manifold is the material-lighting-invariance manifold. For single-illuminant scenes, the illumination for different input RGB values must be contained in the intersection of the corresponding manifolds. The proposed Manifold Intersection method estimates the scene illumination based on calculating the intersection through a Hough-like voting process. Overall, the performance on the two datasets for which camera sensitivity functions are available is comparable to existing methods. The advantage of the formulating the illumination-estimation in terms of manifold intersection is that it expresses the constraints provided by each available RGB measurement within a sound theoretical foundation. It also has the potential to generalize to multi-illuminant scenes.

4: LIST OF CONTRIBUTIONS

The research conducted for this thesis has resulted in two refereed publications:

- Mirzaei, H., and Funt, B., "Gaussian-metamer-based prediction of colour stimulus change under illuminant change," Proc. AIC 2011 Midterm Meeting, International Colour Association, Zurich, June 2011.
- Funt, B., and Mirzaei, H., "Intersecting Colour Manifolds," Proc. Nineteenth IS&T Color Imaging Conference, San Francisco, Nov. 2011 (in press).

My specific contributions are:

- Implementation of the interpolation algorithm for finding KSM colour descriptors.
- Investigation of KSM behaviour under different illumination conditions.
- Investigation of object colour solids of KSM and ADL.
- Implementation of the Gaussian-Metamer-Based colour stimulus prediction.
- Implementation of colour constancy algorithm using direct method and then using look-up table method.
- Experiments on SFU 321-image set and the SFU HDR image set.

5: CONCLUSION

Alexander Logvinenko has recently introduced a new colour atlas based on idealized reflectances called rectangular metamers derived from 2-transition optimal colour stimuli. In summary, the object reflectances and light spectra can be represented in terms of rectangular metamers, which are functions that are a mixture of uniform gray and a rectangular component that takes only values 0 and 1, with at most 2 transitions between 0 and 1. It is possible to specify these functions either by λ_1 and λ_2 as transition wavelengths, or a central wavelength λ and a spectral bandwidth δ. The colour atlas is, therefore, based on idealized reflectances called rectangular metamers specified by 3 parameters: α (chromatic amplitude), δ (spectral bandwidth) and λ (central wavelength). Logvinenko also puts forwards a Gaussian parameterization of his colour atlas. The Gaussians are smooth by definition, and have been used in modelling objects and lights in the literature of colour science. The functions are not strictly Gaussians, but rather are defined on a finite wavelength interval $[\lambda_{min}, \lambda_{max}]$ and in some cases wraparound at the ends of the interval.

In the first chapter of this thesis, we showed experimentally that this colour space has several interesting features including illumination invariance. We considered colour coordinates' behaviour under a change of illumination, and under a change of observer sensitivity spectra, and the superiority of KSM coordinates over their ADL and IG (Inverse Gaussian) counterparts was revealed through experiments.

In the second chapter, we employed KSM as a vehicle for predicting the effect of illuminant change. We first proposed a fast interpolation approach for calculating the

KSM coordinates. A comparison of using KSM coordinates, IG (inverse Gaussians) coordinates, and the von Kries method of colour stimulus prediction substantiated the superiority of KSM in colour stimulus prediction under illumination change. Note that it is not possible to find the IG coordinates for a large portion of the samples. Experimental results confirmed that colour stimulus prediction using KSM coordinates is significantly better than using von Kries scaling, or IG coordinates, in terms of both the angular and CIE 2000 error measures.

Finally, in the last chapter, we proposed a new illuminant-estimation method, taking advantage of Logvinenko's theory. The advantage of Logvinenko's light-colour and object-colour atlases is that they provide a means by which we can enumerate a unique set of illuminant and material spectra that completely covers the entire colour space without any redundancy. In other words, it is possible to generate a complete set of colour-equivalent material and illumination pairs to match any given input RGB colour. The set of such pairs yields a material-lighting-invariance manifold. For single-illuminant scenes, the illumination for different input RGB values must be contained in the intersection of the corresponding manifolds. Our proposed Manifold Intersection method estimates the scene illumination based on calculating the intersection through a Hough-like voting process. Indeed, the illumination-estimation in terms of manifold intersection expresses the constraints founded on the theoretical principles of Logvinenko's colour atlas. Our experimental results on the two datasets for which camera sensitivity functions are available showed that the performance of the proposed approach is comparable to existing methods.

In summary, the Logvinenko's colour atlas, as an illuminant-invariant colour space, demonstrates its power in various areas of colour science. In this thesis I have tried to investigate the usefulness of KSM colour descriptors in colour stimulus prediction and colour constancy as two important concepts of the Colour Vision. However, the applications of Logvinenko's colour space are not limited to these areas.

REFERENCE LIST

[1] A. Logvinenko. An object-colour space, *Journal of Vision,* vol. 9, no. 11, pages 1-23, 10. 2009.

[2] E. Schrodinger. Theorie der Pigmente von grosster Leuchtkraft. *Annalen der Physik*, pages 603-622. 1920.

[3] G. Wyszecki and W. S. Stiles, Colour Science, 2nd ed, *New York e.a.: John Wiley & Sons,* 1982.

[4] P. Nikolaev, A Colour Constancy Model with Continuous Spectral Functions, *Biophysics,* vol. 30, page 112, 1985.

[5] D. MacLeod and J. Golz, A Computational Analysis of Colour Constancy, Colour Perception: *Mind and the Physical World, Oxford: Oxford University Press,* page 205. 2003.

[6] H. Mirzaei, and B. Funt. Gaussian-metamer-based prediction of colour stimulus change under illuminant change, *Proc. AIC 2011 Midterm Meeting, International Colour Association.* 2011.

[7] A. Logvinenko. Object-colour space revisited. *International Conference on Computer Graphics, Imaging and Visualization. CGIV*. 2010.

[8] C. Godau, and B. Funt. XYZ to ADL: Calculating Logvinenko's Object Colour Coordinates. *Proc. Eighteenth IS&T CIC*. 2010.

[9] U. of Joensuu Colour Group Spectral database. *Available online: http://spectral.joensuu/*. Accessed: April 2010.

[10] P. Berens, CircStat: A Matlab Toolbox for Circular Statistics, *Journal of Statistical Software,* vol. 31, Issue 10. 2009.

[11] R.V. Hogg and E.A. Tanis. Probability and Statistical Inference. *Prentice Hall*. 2001.

[12] A. Stockman. Spectral sensitivities of the middle- and long-wavelength sensitive cones derived from measurements in observers of known genotype. *Vision Research*, vol. 40*,* pages 1711-1737. 2000.

[13] J. von Kries. Chromatic adaptation. *In D. L. MacAdam (Ed.), Sources of colour vision* pages 109-119. Cambridge, MA: MIT Press. 1970.

[14] L.T. Maloney and B.A. Wandell. Color constancy: A method for recovering surface spectral reflectance. *Journal of Opt. Soc. Am. A*, vol. 1, n. 3, pages 29-33, 1986.

[15] G.D. Finlayson. Colour constancy in diagonal chromaticity space. *In Proc. Int. Conf. Computer Vision,* pages 218-223, 1995.

[16] G.D. Finlayson. Colour in perspective. *IEEE Trans. on Pattern Analysis and Machine Intelligence,* vol. 18 n. 10, pages 1034-1038. 1996.

[17] G.D. Finlayson and S.D. Hordley. Selection for gamut mapping colour constancy. *In Proc. 8th Brit. Machine Vision Conf. Computer Vision*, vol. 2, pages 630-639. 1997.

[18] G.D. Finlayson, B. Schiele, and J.L. Crowley. Comprehensive colour image normalization. *In Proc. Int. European Conf. on Computer Vision,* pages 460-474. 1998.

[19] V. Cardei, B.V. Funt, and K. Barnard. Adaptive illuminant estimation using neural networks. *In Int. Conf. on Artificial Neural Networks,* pages 749-754. 1998.

[20] G.D. Finlayson, S.D. Hordley, and P.M. Hubel. Colour by correlation: A simple unifying theory of colour constancy. *In Proc. IEEE Int. Conf. on Computer Vision,* pages 835-842. 1999.

[21] G. Buchsbaum. A spatial processor model for object colour perception. *Journal of the Franklin Institute.* 1980.
[22] D.A. Forsyth. A novel algorithm for colour constancy. *Int. Journal of Computer Vision,* vol. 5, n. 1, pages 5-36. 1990.
[23] G.D. Finlayson, M.S. Drew, and B.V. Funt. Colour constancy: Generalized diagonal transform suffice. *Journal of Opt. Soc. Am. A,* vol. 11, n. 11, pages 3011-3020. 1994.
[24] G.D. Finlayson. Coefficient Colour Constancy. *PhD thesis, School of Computer Science, Simon Fraser University, Vancouver, Canada.* 1995.
[25] G.D. Finlayson and S.D. Hordley. Improving gamut mapping colour constancy. *IEEE Trans. on Image Processing*, vol. 9, n. 10, pages 1774-1783. 2000.
[26] G.D. Finlayson and S.D. Hordley. A theory of selection for gamut mapping colour constancy. *In Proc. IEEE Conf. on Computer Vision and Pattern Recognition,* pages 60-65. 1998.
[27] B. Funt. Colour constancy in digital imagery. *In Proc. Int. Conf. on Image Processing,* pages 55-59. 1999.
[28] B. Funt, V. Cardei, and K. Barnard. Method of estimating chromaticity of illumination using neural networks, *U.S. Patent 5907629.* 1999.
[29] V. Cardei and B. Funt. Committee-based colour constancy. *In Proc. IS&T/SID Seventh Colour Imaging Conference: Colour Science, Systems and Applications,* pages 311-313. 1999.
[30] S. Hordley and G. Finlayson, A Re-evaluation of Colour Constancy Algorithm Performance*, Journal of Opt. Soc. Am. A,* vol. 23, n. 5. 2006.
[31] G. Sapiro, Colour and Illuminant Voting, *IEEE Transactions on Pattern Analysis and Machine Intelligence,* vol. 21, n.11, pages 1210-1215. 1999.
[32] K. Barnard, L. Martin, A. Coath, and B. Funt, A Comparison of Computational Colour Constancy Algorithms, Part 2; Experiments with Image*s, IEEE Transactions on Image Processing,* vol. 11, n. 9, pages 985-996. 2002.
[33] K. Barnard, L. Martin, A. Coath, and B. Funt, *Simon Fraser University Computational Vision Lab*, http://www.cs.sfu.ca/~colour/data/colour_constancy_test_images/index.html. Accessed: November 20, 2010.
[34] B. Funt and L. Shi. HDR Dataset, *Simon Fraser University Computational Vision Lab*. http://www.cs.sfu.ca/~colour/data/funt_hdr/ Accessed: November 20, 2010.
[35] B. Funt, and L. Shi. The Rehabilitation of MaxRGB, *Proc. Eighteenth IS&T Colour Imaging Conference.* 2010.
[36] J. van de Weijer, T. Gevers and A. Gijsenij, Edge-Based Colour Constancy, *IEEE Transactions on Image Processing*, vol. 16, n. 9. 2007.
[37] J. van de Weijer, T. Gevers and A. Gijsenij, http://lear.inrialpes.fr/people/vandeweijer/software, Accessed April 2, 2010.